

Chapter 11

Mechanical Testing of Additive Manufacturing Materials



I. Akilan and C. Velmurugan

11.1 Introduction to Additive Manufacturing Techniques

Nowadays, additive manufacturing (AM) matters in large industries and research communities because of its speed, features, and other key features, all of which contribute to the development of superior products [92]. Charles Hull pioneered additive manufacturing methods in 1986 [61]. In 2009, one million AM products were produced by using these 3D Additive Manufacturing (AM) methods. During this time, people are paying more attention to 3D AM products. As a result, every major industry and academic scientist has been working tirelessly to develop AM products. The number of AM products sold in 2019 thus increased by (95%) by almost 5 million compared with 2009 [68]. AMs are also familiar with rapid prototyping and 3D printing technology, which both aid in the production of complex structures through layer-by-layer methods [63]. The traditional 2D method was initially used, but it could not produce sufficient items or construct strong structures. The 3D additive manufacturing process was used. The AM printing system requires the use of high-altitude materials such as polymers, metals, and ceramics [6]. According to the 2017 Wohler's Statement, 97 manufacturing companies worldwide produced and distributed AM systems in 2016 are in Fig. 11.1, with almost half of service providers investing in AM structures that produce metal parts. Because these AM substances were originally based on polymers, academic scientists and their critical effort have focused on the development and improvement of AM systems in all steel substances [76].

This enables investors to help with the development of AM metallic objects that use the net- or mesh algorithms rather than traditional machine or machine tools

I. Akilan · C. Velmurugan (✉)

Department of Mechanical Engineering, Indian Institute of Information Technology
Tiruchirappalli, Tiruchirappalli, Tamil Nadu 620012, India
e-mail: velmuruganc@iiitt.ac.in

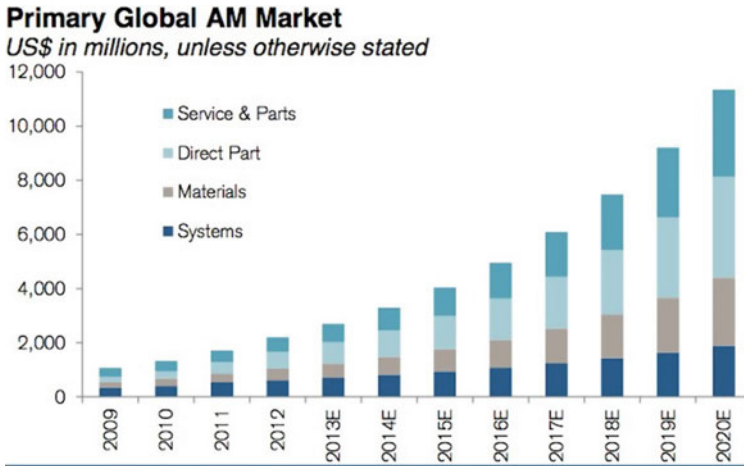


Fig. 11.1 Market growth for AM/3D printing in the future, changes in the aerospace, automotive, healthcare, and consumer markets are expected to grow at a 20–30% annual rate [132]

[92]. The structure of such metal elements is extremely solid and frightening when compared to polymer products. Because of their ability to create complex shapes in the biomedical industry and many other forms, these metal components were very useful in the aerospace industry. These metal components are made of powder or wire-based innovations that are thoroughly assimilated into the basic structure through a heat source and subsequent cooling rate [90]. The technology currently employs less space and is the most reliable in the production of 3D structures of steel, aluminum, and tungsten materials. All these materials are printers that produce rapid prototypes with a small structure and a design of the fabricated part [58]. There are many processes for additive technological methods are shown in the Fig. 11.2, such as high-quality selective laser sintering, electron beam melting, direct metal laser sintering, and selective laser melting, as well as energy deposition techniques such as (laser engineered net shaping, laser metal deposition, direct metal deposition, and so on), all of which include the usage of additive manufacturing fabrication methodologies. In commercial applications, almost all the components of this metal structure are sparingly used. The density, hardness of the surface, tensile strength [41], compressive strength, fatigue, crease, waste stress, and decomposition of printed metal materials is measured using the correct standard ASTM processes and all metal components are systematically produced using 3D fusion technology to determine how well their performance under load is determined [78]. The entire examination process examines AM's mechanical characteristics and test method, and its advantages and disadvantages that are followed by future direction are discussed in the following chapters.

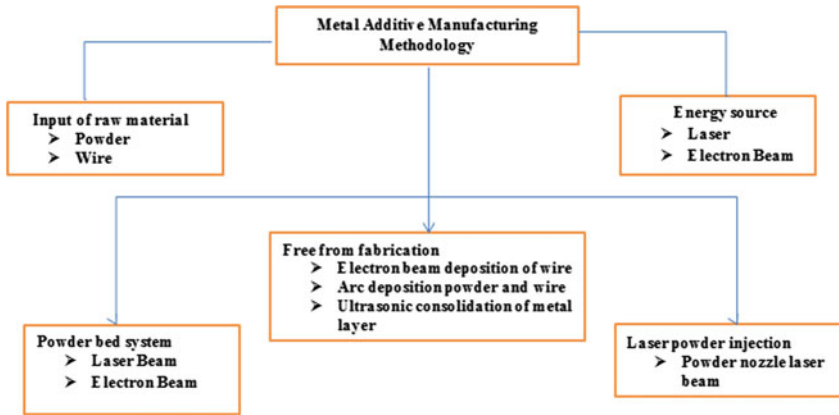


Fig. 11.2 AM processes for metal additive manufacturing

11.2 Classification of Metal Based AM Techniques

The most important characteristics are the type and complete status of the feed, as well as the connection mechanism for the classified AM metal materials. Layered by layering in AM metal, the power input of a laser or electron beam completely melts a powdered feed, or rarely a wire, and transforms it into a firm part of nearly any geometry [48]. The maximum not unusual AM steel approaches are Laser Beam Melting-LBM, Electron Beam Melting-EBM, and Laser Metal Deposition-LMD). For LBM processes, examples include Selective Laser Melting-SLM, Direct Metal Laser Sintering-DMLS, Laser Curing, Laser Metal Fusion-LMF, and business 3-D printing. These all terms are frequently used to describe the LBM process [8]. Metal AM techniques, regardless of their names, all use the same three basic methods: a three-dimensional CAD model is developed on a computer, an imaging device is used, or reverse engineering is used. However, these three procedures differ from LBM, EBM, and LMD in key characteristics, benefits, and drawbacks [20]. These designs are cut into virtually thin layers with a standard layer thickness of D_s 20 μm –1 mm, depending on the metal-based complete AM technology [112].

11.2.1 Laser Beam Melting (LBM)

The material and process risks inherent in each compound production process must be surveyed. The starting materials for Laser Beam Melt (LBM) are permeable and classified by their various size distributions as lung or alveolar (electron fraction or a fraction). This is true for a metal powder that is 15–60 microns larger than the standard particle size distribution [109]. These metal powders have maximum permissible and a limited concentration. Titanium, aluminum, and alloys are reacting with metal that

is of low density. A typical LBM chain is extremely flammable, carcinogenic, and dangerous to the aquatic environment. The specific risk of these hazards must be evaluated for each piece of equipment, material, or process infrastructure.

A galvanometer scanner drives across the deposited powder layer at a (Scanning Velocity- V_s) of up to 900 m/m and LBM beam (P_L) power range of 20 W–1 kW [94]. Single filament radiation beams with wavelengths ranging from 1060 to 1080 nm are released in the nearby infrastructure, which is largely in continuous wave modes in LBM. The standard laser beam interval for the X–Y nozzle jet range between 50 μm and 180 microns, according to the production processes used to produce the selected laser beam output [109]. A sequence, like a strategic structural scan, usually follows the order of each melting path and the melting paths are overlapping at a certain hatch distance. Besides melting exposed material, heat moves volumetric energy from the powder layer to the surface or next to the melting pool. Figure 11.3 depicts the solidification of various melting tracks during and beneath a hard layer. This component is attached to a supporting structure, which is an integrated blade. The support structures are ladle structures that are required to dissipate and adjust the heat in the powder bed, specifically to improve horizontal orientation and surface excess. After preventing the decay of this region, structures to support the removal of the part are added [13]. Besides the substructure, pre-heating the structure can reduce partial deformation by minimizing temperature gradients, resulting in reduced residual stresses during LBM operation. The common setting temperature for the LBM pack of Ti-6Al-4 V components is 500–200 °C. The LBM process is carried out in a closed process chamber with an inert gas atmosphere, which are maintained at less than 0.1% oxygen. The metal powder, when injected with nitrogen or argon into the room, prevents it from melting in contact with the environment. Noble gas flow around the workplace is used to remove secondary process products such as solder sparks and solder spreaders [98].

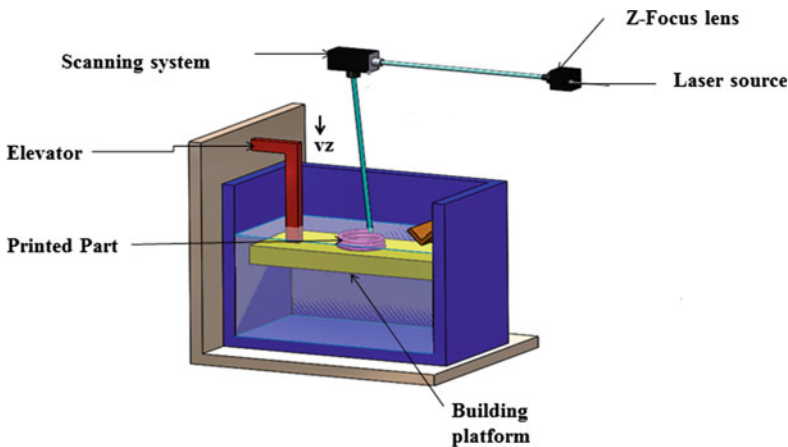
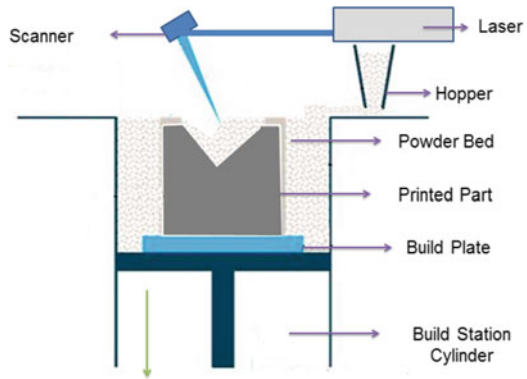


Fig. 11.3 Layer-by-Layer LBM process

Fig. 11.4 Systematic diagram laser metal fusion



11.2.2 Laser Metal Fusion

The LMF is also known as metal 3D printing. The know-how in metal 3D can picture the interest of designers of fabrics, but it takes more effort to print a 3D part. A 3D model, typically 20–100 microns thick and using specialist software, is “sliced” into thin layers. All components must be optimized for fusion efficiency, location density, and heat management. Finally, as shown in Fig. 11.4, the part is built layer by layer using a cultured laser fusion method. A layer of metal powder is used to connect the cross-phase geometry to the plate, which is then driven by the optical scanner using a laser beam [32]. The plate is reduced after treatment, and it adhered in the next particle layer to. It follows a series of steps until the part is finished. This can take longer depending on the size, thickness of the components, materials used, laser energy, scan velocity, spot dimension, and other variables [107]. Some post-processing steps may be required when removing a partition from the system. After heating, removal of hips and integrated panes, production of any interface layers, and final surface processing, such as bell surface processing (including high-density hips). In many industries, metal 3D printing has already affected such as dental, medical or marketing prototyping, including titanium for hip joints, cobalt chrome for dents and bridge steel, among other examples. Even though the parts are mass-produced, each one of its materials has a unique characterization [30]. In fact, the aviation industry has since shifted toward the production of 3D printed prototypes. The ability to create simple and flexible bionic structures has enabled structural geometries which were impossible to implement with traditional manufacturing methods.

11.2.3 Electron Beam Melting (EBM)

Electron beam melting-EBM is a method of melting powdered metal layers using electron beams. Arkham, a Swedish company, first introduced EBM in 1997, making it ideal for light, long-lasting, and dense finishing elements, including space,

medicine, and security, are the most common applications of technology. Laser Powder Bed Fusion (LPBF) combines metal particles using electron beams to create layer-by-layer, desired areas [40]. The heat source used is the primary distinction of LPBF technology. Here, EBM technology makes use of electron beams generated by an electron gun. Under vacuum, the latter removes electrons from the building tray of a 3D printer and quickly converts them into a layer of metal powder, as shown in Fig. 11.5. These electrons can then choose the powder and produce some of it (2017). The drive removes a component from the machine at the end of the manufacturing process and uses a brush to clean the blister or dust. This can remove print media and partitions from the box (if needed). After printing, working, and polishing surfaces in contact with other parts. The stress created by the manufacturing process may cause several hours of heating in the oven. For the electron beam to function properly, all production must take place in a vacuum. This prevents the powder from oxidizing when heated. Most insoluble powders can be reused after the manufacturing process is finished. Manufacturers, particularly in aeronautics, understand the appeal because from the materials purchased only 20% is used for the unalterable part, with the rest being separated and recycled [57].

Today's most common materials are titanium and chromium-cobalt alloys, limiting the range of Arcam compliant products. Users must first complete the additional training and get permission to use the machine as needed before using or testing another product. Because the powder is more granular, electron beam melting produces components faster than LPBM, but the process is less accurate and the cover quality is lower [15]. The electron beam is separated, allowing dirt to be heated in multiple locations at the same time and speed up production. When controlling heat dissipation before melting and reducing the need for reinforcement and production help [69]. At the fine powder level, the electron beam is broader than the laser beam,

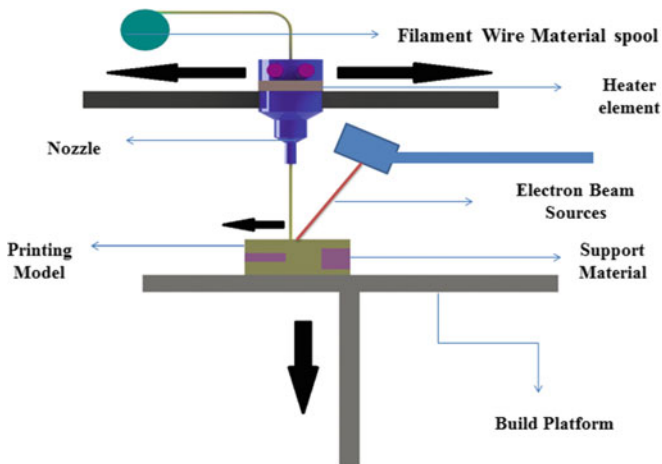


Fig. 11.5 EBM 3D printed process diagram

which affects accuracy. The EBM (Q20 Machine) has the largest construction size, with a circle of 110 cm of 38 cm.

11.2.4 Laser Metal Deposition (LMD)

Laser metal deposition-LMD is a type of metal production process. The term “Laser Metal Deposit,” abbreviated as LMD, is widely used throughout the universe. LMD is also known as “Direct Metal Deposition-DMD” or “Direct Energy Deposition-DED”. LMD is a new technology that combines powdered components and laser drilling to achieve greater accuracy [89]. As a result, this process continues to develop in significant applications such as aeronautical and medical regardless of performance and acceptance criteria in those industries. In terms of repairs, the low thermal input allows an automatic change of complex spaces to create a smaller thermal surface. The layer’s overall microstructures, as well as the residual stress caused by the steep thermal gradient, are anisotropic [79]. These effects have a negative impact on the machine’s component properties. Because there are so many process variables in LMD today, estimating the properties of manufactured LMD components is extremely difficult. Thermal history is a cumbersome subject that can be altered by different factors. Depending on the material structure, the process metrics can have a complex impact on the microstructure [104]. Despite the significant benefits of LMD, a thorough understanding of the process structure and asset relationships should place a special emphasis on the impact of powder properties. The geometry, structure, and grouping of sediments are critical for a variety of service applications, depending on the process variables, the metal, and the resulting mechanical properties [79].

DLMD is a quick tooling process that uses a laser to liquefy the metallic sediments into pieces and molds. In this method, which is comparable to traditional rapid prototyping, metal powder and tool steel melt faster than plastic polymers. The DLMD tool can create or reassemble genuine finishing materials such as metal materials of aluminum parts, molds, and dies. It always generates a new CAD drawing area or reconstructs an existing component. To extend the molten pool, a small stream of molten tool steel is injected into it. Layer builds the solid metal element layer by moving the laser beam back and forth under CNC control and locating the controlled form using a computerized CAD design. The components are consistent, well structured, of high quality, and well equipped. By combining several metal powders in the melting pool, the alloy can be replaced by DLMD [59].

Direct Laser Metal Sintering-DLMS and Selective Laser Melting-SLM are high-intensity laser sintering techniques that are also known as Direct Laser Metal Fusion (DLMF). A metal part is included in the computer-aided design file, and the bed is covered in metal powder. This technology improves the SLS process by layering metal powder to create true three-dimensional parts. This technology allows for the direct production of human implants from computer-aided design models with minimal processing time. The primary goal is to produce completely high-density

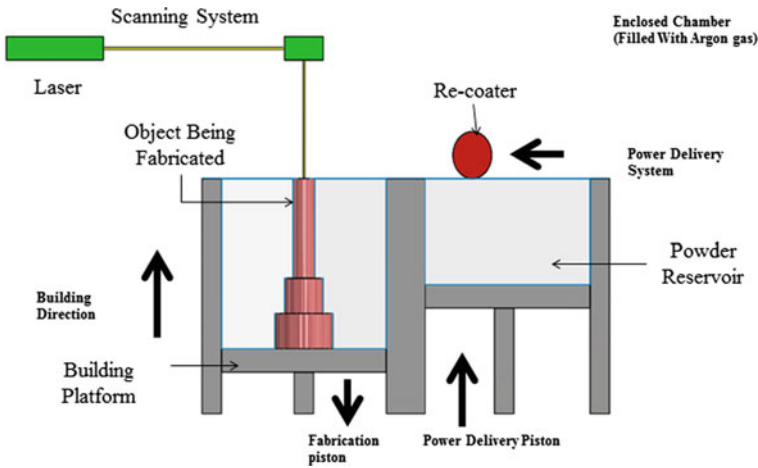


Fig. 11.6 Experimental setup of selective laser melting (SLM) process

metal parts [34]. Figure 11.6 shown traditional SLM systems use high-precision beams with a diameter of only 0.03 mm and Z-axis steps of only 0.05 mm, with no complex metal components. If the high-power laser beam is heated in layers of 20 to 40 μm without a binder or fluxing agent, bronze, steel, 316L steel, titanium, or Al-30% are possible. DLMS can improve a wide range of applications, such as aircraft, interfaces, and frames. Using costly materials with complex devices, as well as 3D metal printing, is beneficial in the medical field. Customer requirements are typically highly specialized/precise [83].

11.3 Additive Manufacturing of Metal Based Products

The success of AM powder sheet fusion is critical for high-quality metal powder and wires. Titanium and its alloys, stainless steel and alloys, aluminum alloys and different metals in the form of a powder, depending on processor requirements such as copper(cu), nickel chromium and cobalt alloys, found less alloys and highly expensive metals like gold, platinum, palladium or silver, are the focus of this section [78]. Wire feeds are also available in a variety of materials, including iron and carbon—its alloys, including pure metals substance such as Titanium-Ti, Tungsten-W, Niobium-Nb, Molybdenum-Mo, and Aluminum-Al. However, not all materials have been used in additive manufacturing, but the metal powder can be qualified for a specific purpose most times and with the right equipment.

The layer thickness and partial sphere geometry distribution of gas atom particles typically range from 10 to 50 μm . This is a common feature of metal powders suitable for AMs. Tensile strength, hardness, and lengthening are important material characteristics that are frequently used to determine the right material [48, 28].

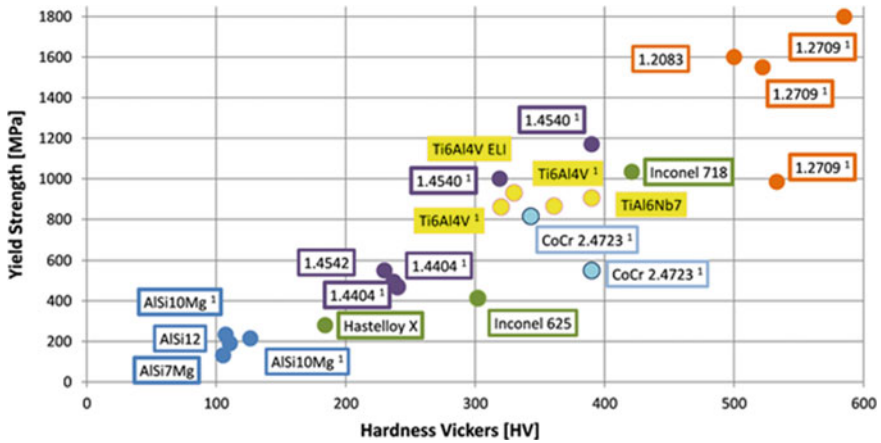


Fig. 11.7 Mechanical characteristic of metal products

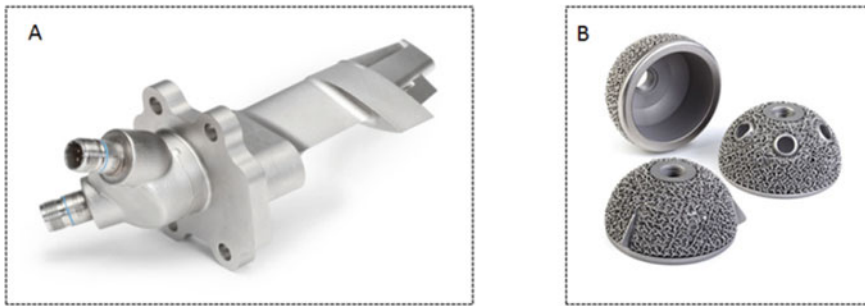


Fig. 11.8 a 3D Inlet sensor housing unit in jet motor b 3D acetabular cup [78]

The image (Fig. 11.7) depicts some of the various alloys and their detailed output yield strengths. Based on two mechanical properties, the user can select the object using this diagram. Yield strength was calculated using the best value found on the manufacturer’s datasheets [96].

11.3.1 Titanium and Its Alloys

Non-workable titanium alloys are traditionally available and have a variety of manufacturing applications. It is available in one to four grade classes, depending on the quality of the application. Even though all grades have exceptional corrosion resistance, ductility, and weldability, grade one is far superior to grades II, III, and IV are powerful. Level II titanium is the best combination of design and strength [25]. Only a few industries use condenser pipes, high heat exchangers, turbojet jet

engines, aviation, and marines. Titanium grade-II is used in biomedical implants and prostheses. In precious metals such as titanium and other alloys, reducing waste is an enormous benefit. Shorter lead times and more constrained manufacturing flows are becoming more prevalent [25]. According to the well-known laser and electron beam AM methods, Boeing estimates that using fully 3D-printed titanium components could save the 787 Dreamliner \$3 million. GE has developed miniature titanium of 3D inlet sensor housing unit in Jet Motor as shown in Fig. 8a. In a NASA-tested demonstration of that engine, fluid hydrogen was extracted at 696.15 K and fuel burned at 6273.15 K [58].

The titanium ASTM grade five casting alloy is a combination of alpha–beta alloy with a Young module of 0.1–0.130 Tera pascal. Huge bone implants have such a young modulus, but the level of porosity can be reduced as well as porosity can be controlled, which are shown in Fig. 8. With the help of EBM, titanium composites are used to manufacture a variety of industrial essentials, such as turbine blades, latches, screws, rings, discs, acetabular cups, hubs, and ships [78]. High-performance engine parts like gear trains and piston rods employs Titanium alloys for its production. Metal is a viable option in medical applications because of materials with high biocompatibility, such as cobalt chromium and titanium, especially when there is direct metal contact with bone or tissue [93].

11.3.2 Stainless Steel

Stainless steel has many tremendous mechanical properties in additive manufacturing, including robustness, design, and tensile strength to a wide range of automobile, light industries, food production, and therapeutic diagnostic application [108]. EBM technology employs stainless steel powder to create super-strong and dense waterproofing components for aerospace applications such as jet engines, rocket motors, and nuclear power plants [36]. The 2016 review of literature looks into the use of low-carbon steel in EBM machines, such as those used to develop nuclear energy pressure vessels. Following that, 316L steel was chosen because of its softness, strength, and resistance to corrosion. Most AM’s literature focuses on 316L quality austenitic stainless steel, which is a popular choice for a variety of industrial applications as shown in Fig. 11.9 [31]. However, if any successes or difficulties in various properties are reported, other types of austenite steel, such as grades 304 L, will be investigated. The most significant difference between 316 and 304L chemical composition is that 316L contains close to 2 with % Mo to improve corrosion resistance [52].

Tool steels differ significantly from structural steels in that they are used to making tools that are resistant to wear and hardness. “Tool Steel” believes such steel contains at least 0.7% carbon. However, the maraging steel compositions are Fe-65, Ni-18, and C-80%, and are established in the tool and die-making industries because of their increased unique strength, fractural hardness, and weldability. Molding, high pressurized die-casting, stumping and protrusion die-cutting, and plastic injection

Fig. 11.9 Air brackets of 316L austenitic stainless steels



are some of its tools [62]. Steel is a powder that can be used in a variety of ways in compliance with additive manufacturing solutions like SLS or DMLS. Steel is more accessible on the 3D printing market than other metals and it can be used in a broad range of alloys, making it even more attractive to specially designed through industry requirements. Steel metal has been the most frequently used material in the AM because of its high mechanical properties. According to the investigation, the number of powdered steel supplies used in industries such as aerospace and automotive increased by 48% in 2018 [43].

11.3.3 Aluminum and Its Alloys

DMLS will be used to sinter aluminium, and a Selective Laser Melting process will be used to melt it (SLM). As a result, it can be applied to walls with layer thicknesses ranging from 25 to 50 microns. As shown in Fig. 11.10, the reusable jig parts have a rough, matte finish that distinguishes them from standard milled aluminium parts. 3D-printed aluminium parts are mostly used for automobile parts and, in particular, racing

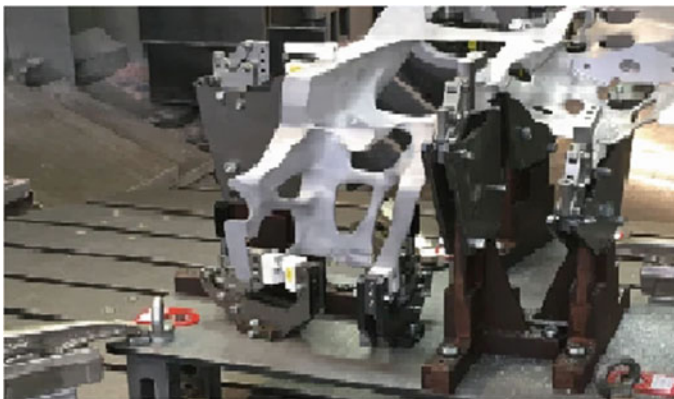


Fig. 11.10 Reusable jig for automobile car parts [18]

car components due to their good mechanical properties of lightweight, strength, and impact under load conditions [18]. They have excellent strength-to-weight ratios and are resistant to excessive wear and corrosion. The aluminum alloy powder has a significant advantage over other metal powders commonly used in PBF because it provides higher training levels. Because of the geometrically complex structures used in additive manufacturing, additional weight reduction has been frequently possible with little or no loss of strength or overall performance [18].

The strength of aluminum alloys with a thin grain microstructure and grain dimensions is like those of forged counterparts. It is ideal for 3D printing with aluminum alloys because of its excellent fusion properties. Aluminum cast alloys are often used for the AM category PBF, whilst wrought aluminum alloys should be used in DED processes, sheet, and film for SL types of processes. Although most research and development of PBF alloys of aluminum is done by melting alloys that are well suited to the conditions of heating and cooling in electron beam processing, manufactured alloys such as 6061 and 7075 have long grain structures that allow PBF processing [2, 4, 112]. HRL labs recently solved this problem by incorporating zirconium hydride nanoparticles into powders 7075 and 6061. Nanoparticles act as nucleating sites for the desired alloy microstructure during PBF processing, preventing hot cracking and resulting in high-strength aluminum alloy AM components [51].

11.4 Metallurgical Characteristics of the AM Metallic Component

The microstructures of AM-made metals are distinct because of the AM process. A column with a high grain orientation dominates the grain structure. The creative process is broken down into phases, each of which focuses on a different topic. Axial grain and grid fluctuations can occur because of the material's subsequent heat and cooling cycles. In theory, the scan method can control the microstructure, and recent research has made significant progress in this area. Porosity refers to all processes that can be handled using DED, LM, or EBM to optimize less than 1% of process parameters.

11.4.1 Microstructural Properties on AM (PBF) Components

Several studies have been conducted to investigate the relationship between PBF microstructure and process parameters. Most scanned powder melts and thickens at higher processing temperatures, but PBF manufactured components keep some porosity. Figure 11.11 depicts the Ti-6Al-4 V microstructure following SLM processing [111]. Two parameters that influence the granular microstructure of PBF regions are temperature gradient and interface velocity of solidification. Column

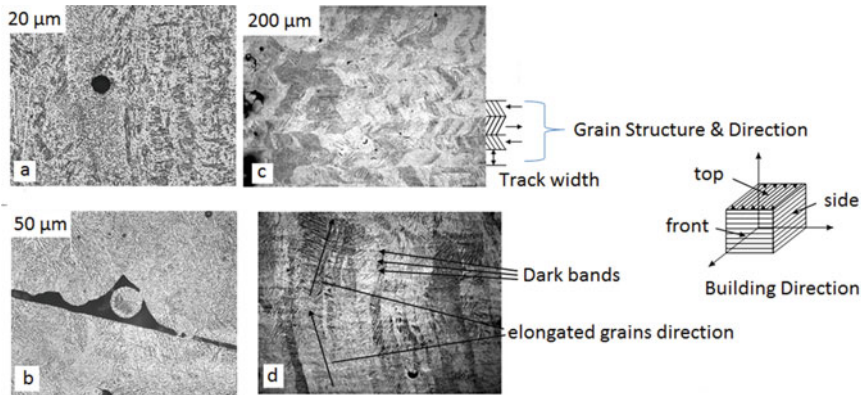


Fig. 11.11 SLM-built Ti-6Al-4 V microstructures; (a-porosity caused by trapping gas), (b-inadequate heating), (c-top view) and (d-side view) [72]

grains form when the interface speed is slow and there is a large temperature differential. In contrast, small temperature gradients and chief contact speeds result in equal grains. The grain conversion can be calculated using the Hunt dendrite growth model [40, 84]. Built their strategy around this approach, solid maps are created using a variety of nickel alloys for Inconel 718 and RS5 alloys. Sames et al. [74] have developed an EBM processing window. Their findings suggest that these two parameters can have a significant impact on the grain development of Arcam Inconel 718. The scan speed, laser, or E-beam feature may affect the temperature gradient and the speed of the interface. Several recent papers have addressed the use of process design to manage the microstructure. Later examined the processing window to determine which grains in the column were the best. Mechanical qualities of materials created by SLM or EPM are critical for their applications.

11.4.2 Microstructural Properties on AM (DED) Components

Ziętala et al. [114] we are the first to present a thorough examination of the microstructure of LENS manufactured regions. They were specifically used in their research to compare the tensile properties of the materials created. The rate of local solidification in the melt pool, the temperature differential at the solid–liquid interface, and the rate of refrigeration all influence the solidified microstructure. Changes in these values can cause one of three structural morphologies in Ti-6Al-4 V/DLD components. To create products with exceptional mechanical properties, the effect of process parameters on the microstructure must be efficiently optimized and managed. The Ti-5Al4V macrostructure is shown in the Fig. 11.12 comprises columns of prior-b grains stretched toward solidification (build) [11].

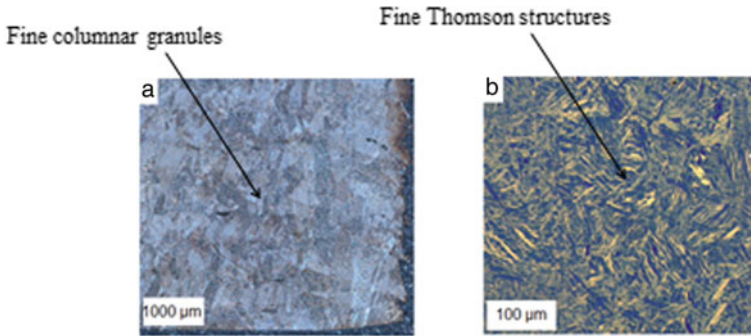


Fig. 11.12 Ti6Al-4 V generated by a LENS [11]. **a** Macrostructure. **b** Microstructure

A melt pool's border is a superstructure filled with a cellular structure and cellular spacing as small as 1 mm. Larger melting pools are found in large 100 mm 140 mm grains and a nearly mono crystalline LMD structure than in LBM [37]. According to Morrow [55] larger melt pools coarsen the microstructure and texture because of slower cooling rates.

Smaller melting pools form fine-graining microstructures that are weakly expanded by increased replacement. After AM manufacturing, austenitic steels (such as 304L and 316L) frequently exhibit entirely austenitic microstructures, particularly LBM. D-ferrite was found in as-machined 316L samples as shown in Fig. 11.13, and it converts to extent after a 2-h heat treatment at 1150 C and cooling with air. Precipitation has been observed in stainless steel (17-4 P_H), maraging steel (18-Ni300), and martensitic steel grade AISI420 (X46Cr13). Because of the changing thermos-conductivity of the gas, even minor changes in the cover gas in LBM can cause significant changes in phase composition because of the behavior's compatibility with freezing settings [10, 72].

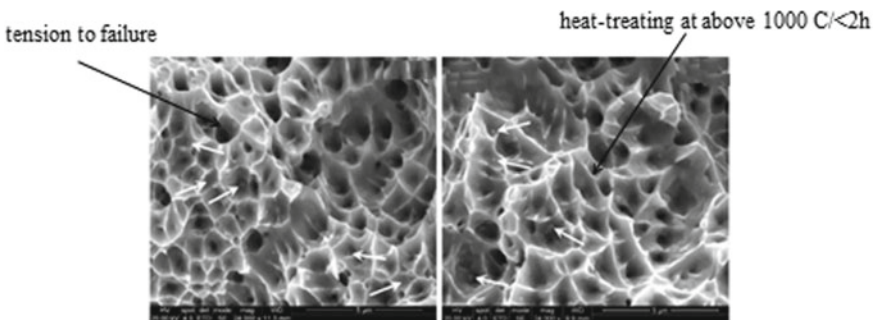


Fig. 11.13 316L stainless steel fracture surfaces [55]

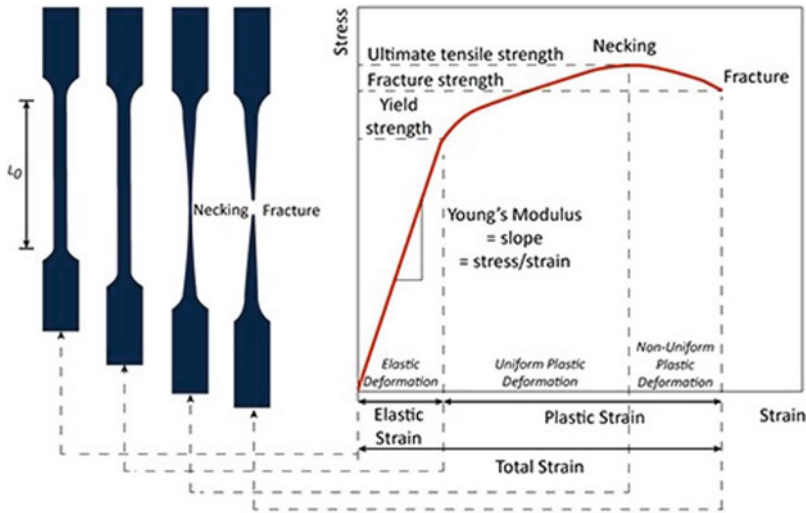


Fig. 11.14 ASTM standard testing methods for AM metallic materials

11.5 Standards of Mechanical Testing

As technology advances and enters the market, the need to comprehend technical jargon and system features grows. Metal additive manufacturing has progressed to the point of commercialization. The dental and aviation industries, for example, have moved to commercial manufacturing and now require material belongings standards, inspection methods, and other data. Added substance Manufacturing is changing ventures across the globe and a different scope of organizations are seeing the large number of noteworthy freedoms that the innovation offers. There are still numerous difficulties ahead to make this innovation a supported achievement [97].

The solid connections between the boundaries of assembly and the material properties require special consideration in contrast to the standard measuring measures for metal molding. It is also necessary to consider the impact of different machine frameworks and conditions, resulting in various characteristics as shown in Table 11.1. Most major organizations currently use AM to create end-use components in view of the lack of guidelines, make own interior arrangements of materials and operating rules. The improvement of measurement information and the development of standard specialized guidance are therefore of outrageous importance. The Plan Guidelines will help further recognize that AM does not make use of the maximum capacity of additive manufacturing in the vast majority of current CAD devices [54].

Two fundamental worldwide establishments, ISO (International Standardization Organization) and ASTM International, universally plan, create and distribute principles identifying with AM. The European Committee for Standardization (CEN) has likewise shaped normalization boards of trustees for AM on a territorial level. There are a few public exercises identified with normalization and rules. These incorporate

BSI (British Standards Institution) and France’s AFNOR/UN (Union de Normalization de la Mécanique). In Germany, the public principles body DIN (Deutsches Institut für Normung) distributes guidelines identifying with AM in collaboration with VDMA (Verband deutscher Maschinen-und Anlagenbauer) and VDI (Verein Deutscher Ingenieure) [82]. ASTM International set up the F42 Committee on the

Table 11.1 Metal part mechanical testing [97]

Typical designation	Typical name	Remarks
ISO/ASTM 52,900:2015	Creates and defines phrasing for use in added substance manufacturing (AM) innovation	This applies the added substance-forming rule and along these lines constructs actual 3D calculations by the progressive option of material
ISO/ASTM 52,921:2013	Standard wording for added substance producing—Coordinate frameworks and test systems	The terms covered include definitions for machines/frameworks and their organizing frameworks, as well as the area and direction of components
ISO 17296–2:2015	Added substance producing—General standards—Part 2: Overview of cycle classes and feedstock	Shows how extraordinary cycle classes use various materials to frame the math of an item This standard builds up the preparation for the Additive Manufacturing measure. It is anything but an outline of existing cycle classifications, which are not and cannot be finished as innovations arise
VDI 3405	Basics, definitions, and methods of additive manufacturing and fast manufacturing	Explains the monetary available additional substance manufacturing measures, Works with a superior evaluation of different additional substance generating measures, Establishes the quality limitations for different added ingredient production measures, Recommends the scope and content of testing and supply agreements
ISO 17296–4:2014	Added substance fabricating—General ideas—Part 4: Data preparing outline	Enables the determination of an appropriate arrangement for information trade It shows the most recent developments in the addition of material to 3d computations, It tracks existing document designs that are being employed as a part of contemporary occurrences, and Facilitates international standard adopters’ understanding of key points for information exchange

(continued)

Table 11.1 (continued)

Typical designation	Typical name	Remarks
ISO/ASTM 52,915:2016	File Format Specification for Additive Manufacturing (AMF)	<p>This record details Additive Manufacturing File Format (AMF), a configuration for commercial applications to satisfy the current and future needs of innovation in additional substances</p> <p>The need for preparation, display and forwarding for the AMF is defined in that archive. At this time, the perfect adherence to the extensible labelling language (XML)(1)2 in a structured electronic organization maintains standards for acceptable interoperability</p>
ASTM F2924	Added substance Manufacturing Standard Specification PBF of Titanium-6 Aluminum-4 Vanadium	<p>This standard relates to titanium-6aluminum-4vanadium (Ti-6Al-4 V) segments manufactured additively using a full-dissolve powder bed combination, such as electron bar softening and laser liquefying. It displays the segment configurations as well as the feedstock used to produce Class 1, 2, and 3 segments, as well as the component microstructure</p>
ASTM F3001-14	Additive Manufacturing Specification ELI (Extra Low Interstitial) Titanium-6 Aluminum-4 Vanadium with PBF	<p>The standard addresses material characterization, request data, manufacturing plan, feedstock, measurement, synthetic structure, microstructure, mechanical properties, warm handles, Hot Isostatic Pressing, measurements, and weight. These lay the groundwork for the usage of complete liquid PBF for additively manufactured titanium-6 aluminum-4vanadium with extra low rates (Ti-6Al-4 V ELI)</p>
ASTM F3055–14a	Standard specification for PBF manufacturing additive nickel alloy (UNS N07718)	<p>This decision applies to UNS N07718 (2.4668–NiCr19NbMo) segments produced additively utilizing a full-soften powder bed combination, such as electron bar dissolving and laser liquefying. These cycles produce products that are widely utilized in applications that need mechanical characteristics, such as machined forgings and fashioned objects</p>

(continued)

Table 11.1 (continued)

Typical designation	Typical name	Remarks
ASTM F3056–14e1	Powder Bed Fusion Standard Specification Nickel alloy manufacturing additive (UNS N06625)	ASTM F3056–14e1 covers additively produced UNS N06625 (2, 4856–NiCr22Mo9Nb) components employing a fully dissolved mixture of powder beds such as electron pillar softening and laser liquefying
VDI 3405 Part 2.1:2015–07	Speedy creation strategies—LBM of metallic parts; Aluminum composite AlSi10Mg material information sheet	VDI 3405, Part 2-made use of the test techniques and tactics. Because this load of approaches and methods corresponds to recognized industry norms, the trade name values and customary assembly measures can be compared
ASTM F2971–13	Standard practice for the reporting of additive manufacturing data for test specimens	Test example representations and test reports standardization To help creators normalize information bases for AM materials Aid material deactivated by testing and evaluation Capturing AM examples for property limit execution to empower high-performance displays and other computational methods
ASTM F3049–14	Standard Guide for Characterizing the Properties of Metal Powders Used in Additive Processes	This document aims for the provision of current standards for metal powder for additive manufacturing for purchasers, suppliers and manufacturers. It is linked to several current standards for determining the cleanliness of new and used metal powders
ISO 17296–3:2014	Manufacturing additives—General concepts—Part 3: Principal features and appropriate testing procedures	ISO standards 17,296–3:2014 are required when testing components created using additive manufacturing techniques. It shows the components’ essential quality characteristics, determines appropriate test techniques, and proposes test and supply arrangements in terms of degree and substance. The main guidelines are machine manufacturers, feedstock suppliers, machine customers, part suppliers, and customers

Additive Manufacturing Technology in 2009. Public workouts began in Germany and the United Kingdom around the same time. In 2011 and July 2013 ISO started its TC 261 exercises and the two associations, ASTM and ISO, established a Joint Improvement Plan for Guidelines. In 2018, the Standardizing Roadmap for AM was distributed under a joint effort between ANSI and America Makes, the Additive Manufacturing Standardization Collaborative [97].

Substance was added Manufacturing is a form of invention that both enables and animates growth. AM is rapidly evolving, with major investments being made all over the world. We are just looking into the many possible results of AM innovation. It is critical to acquire knowledge and benefit from teamwork in order to exploit maximal capability. It is advantageous to employ new item strategies. Item creators characterize the specific requirements of products based on demonstrated manufacturing measures. It is critical to have standards coordinated within the item improvement measure in order to meet requirements such as material characteristics and quality control difficulties. The application of principles is required for the evolution of innovation. Global collaboration is undeniably beneficial to everybody, while a conflict over values would be detrimental. The shared aim should be a collection of universally applicable ideas. A global handbook to AM principles might be a step in the right direction. Existing principles, for example, might be modified for AM to speed up this interaction. The combined endeavor of ASTM International and ISO to create and successfully communicate a first principle agreement is a prime example of collaboration. The ISO/ASTM Guidelines have the potential to shift the next phase to CEN standards.

11.6 Mechanical Properties of Metal AM Components

This section discusses the mechanical characteristics of metal AM components, such as ductility, strength, and anisotropy, with an emphasis on the relationship between construction and properties. The primary goal of AM process optimization is to produce materials with a high density, which is typically higher than 99.5% [3]. The volume energy used affects partial density. Because of the irregular vacuums caused by insufficient energy consumption, the material remains unmolten, resulting in a reduction in density. When there is a surplus of input energy, the dynamics and density of the melting pool increase [99]. Straightaway structure deformity in Ti-6Al-4 V was caused by scarce melting, according to Vilaro et al. [95] and Carlton et al. [21]. These events were typically longer (10–15 cm) than the vents discovered previously.

Qiu et al. [65] discovered that the residual porosity of LBM-produced Ti-6Al-4 V was primarily spherical. They claimed that most voids were not filled with gas because they were not reopened in subsequent heat treatments after the preceding HIP. Yasa et al. [106, 115] Proposed a collage strategy to reduce the residual porosity of 316 LBM from 0.77 to 0.036% by cooling a layer twice time before implementing the next metal powder layer. The 3D printing test determines how a 3D printed material will

withstand a load and provides information about its quality and mechanical conduct. ASTM-based testing assists manufacturers in ensuring that their processes meet industry standards. Mechanical tests can aid in the investigation and development of a new or altering material, manufacturing process, or high-quality product. The outcomes of various processes, such as DED-EB, DED-L, PBF-EB, and PBF-L, are addressed.

11.6.1 Hardness

Hardness testing is an effective method for demonstrating that metal AM components have limited mechanical strength. Table 11.2 summarizes the hardness properties of several AM metal composites. The current study found a link between Vickers microhardness and AM titanium composite microstructural highlights, as well as a relationship with the Hall–Petch. Several studies were conducted to ascertain the effect on cross-sectional hardness estimates. A previous study discovered that metal component size AM had no effect on micro-hardness, most likely due to insufficient warm separation. A recent study evaluated the hardness attribute on a cross-sectional region. Because of microstructural coarsening, the micro-hardness decreased as the cross-sectional area increased. Because the portion with the thicker cross section has more conspicuous heated information and slower cooling rates, microstructural coarsening occurs. In addition, the study found that differences in 2D planar estimations had an impact on micro-hardness due to contrasting heat movement. Further research was carried out to assess the impact on durability of the manufactured height. However, the results of these studies were contradictory. For example, Hrabec and Quinn [39] have found that Vickers' structural micro-hardness values are contrasted with no critical contrasts of up to 25 mm from the substrate while Tan and colleagues have

Table 11.2 Hardness characteristics of different metal AM parts

Process	Material	Microhardness (Hv)	Distance measured from the substrate (mm)
EBM/Arcam [39, 88, 97]	Ti-6Al-4 V	347	2–25
	Pure Cu	57–88	NA
	AlCoCrFeNi	400–500	0–16
	SS316L	184 ± 11	2
	IN718	241 ± 12	2
	Al-8.5Fe-1.3 V-1.7Si	153 ± 2.5	NA
SLM [38, 42, 113]	Ti-6Al-4 V	360	NA
	SS316L	213–220	NA
	IN718	365	1.3–2.4
	Al-8.5Fe-1.3 V-1.7Si	135–175	NA

found that Vickers' structural micro-hardness values do not differ from any critical contrast between the substrates up to 25 mm.

Tan et al. [88] concluded that Vickers micro-hardness decreased as the tallness of EBM Ti-6Al-4 V increased. The heated conductivity increases the rate of cooling of the treated steel substrate. The microstructure of the base site was superior to that of the top site. Nonetheless, Wang et al. [97] investigated the pulley's micro-hardness. According to the study, the value of micro-hardness increased as assembly size increased. Many people claim that the variability in hardness estimates is caused by warm data from a specific stratum. Compared to a smaller transversal area, the greater transversal area would result in a warmer contribution and in a variety of final microstructures. Future improvements to change the cycle limits in the cross-sectional area could help to simplify this heterogeneity of hardness.

11.6.2 Tensile Properties of AM Developed Metal Components

In the manufactured state of the AM, the tensile strength of existing steel grades frequently meets the specific requirements for industrial applications. Grain refining increases yield and tensile strength significantly. In terms of ductility, lower porosity (0.1%) results in a malleable fault mode with lengthening values compared to the material used. High remaining porosity of 2.4%, on the other hand, results in flexible modes with significantly lower elasticity [21]. Table 11.3 compares Yield Strength- Y_S , Ultimate Elastic Resistance- U_{TS} , and Failure Elongation- E_L to the reference qualities of the materials produced for the selected grades of steel, aluminum, and titanium for the various AM technologies derived from literature [23]. Stability properties differ widely in LBM, which depends on the tensile test, which can be determined by selected parameters of processing and post-processing conditions under various loads. In the AM-microstructure/yield correlation, the tensile properties of Al alloys compare favorably to those of AM-constructed steels. AM techniques produce granular configurations that primarily or solely increase the strength of the manufactured state [28].

The actual coarsening of smooth grains during the hardening period of a manufactured additive AlSi10 Mg alloy, which counteracts the later impact and maintains a constant yield strength as the manufactured part (Table 11.3). Mg was lost during AM production for AA 2139 (Al-Cu, Mg), which reduced precipitation and thus output strength. When attempting to maintain a thin grain structure while producing an unnaturally aged precipitate, an LBM manufactured scan-based alloy produces the best results [2]. Because titanium is a great material for EBM, LMD, and LBM, the complicated interrelationships among various AM methods, specifications, and the resulting fatigue and tensile properties, particularly for Ti-6Al-4 V, are widely preferred for metals and alloys (2015).

Table 11.3 Tensile properties of different metallic materials are generated AM process

AM Techniques	Materials	Reference by	EL [%]	UTS [MPa]	YS [MPa]
LBM	Steel	Carlton et al. [21]	44 ± 7	705 ± 15	590 ± 17
LMD	Steel	Yadollahi et al. [102]	36 ± 4	640 ± 20	410 ± 5
LBM	304L Stainless	Elghany and Bourell [1]	25.9	393	182
LBM	18Ni-300 Maraging Steel	Yasa et al. [106]	1290 ± 114,	1214 ± 99	13.3 ± 1.9
LBM	AlSi ₁₂	Prashanth et al. [64]	3	380	260a
LBM	AlSi ₁₀ mg	Monteiro [53]	6.2 ± 0.4	328 ± 4	230 ± 5
LBM	AlMg ₁ sicu	Fulcher et al. [29]	E	42	E
LBM	AlMg _{4.4} Sc _{0.66} MnZr	Schmidtke et al. [75]	16	530	520
EBF	AA 2139 (AlCu, Mg)	Brice et al. [16]	E	430 ± 8	321 ± 26
EBM	Ti-6Al-4v	Yamanaka et al. [103]	28.5 ± 0.5	475 ± 15	377 ± 10
LBM	Ti-6Al-4v	Vilaro et al. [95]	8.2 ± 0.5	1140 ± 10	1040 ± 10
LBM	Cp Ti (Grade 2)	Ambrogio et al. [9]	20	345	280
LMD	Ti-6.5Al-3.5Mo-1.5Zr-0.3Si	Zhai et al. [110]	7	1042	990
PDF	Inconel 625	Martinez et al. [50]	58	900	380
DED	Inconel 718	Blackwell [12]	38	1000	650
DED	Inconel 625	Wang et al. [96]	E	722 ± 17	42.27 ± 2.4

Table 11.3 shows that AM processes for Cp-Ti result in higher output strengths and ductility than sheet Ti processes (20%). When test conditions, such as LBM's extremely high melting temperature, produce a very thin martensitic (Alpha) microstructure, the greatest strength will be achieved. Grain refining improves ductility and yield. LMD has lower output strengths than LBM or EBM due to lower cooling rates (Table 11.3), and the resistance of tensile failure to the testing parameters varies significantly. Moisture levels have increased, but ductility has decreased [22]. Furthermore, it is related to the increased α -martensitic, remaining permeable,

and residual stresses in the flexible mode of as-made AM Ti-6Al 4 V. As shown in Table 11.3, computer imaging has been used successfully to detect material structural limitations, and additive mechanical flexible fracture software has been used to show the effect of these limitations on EBM Ti-6Al-4 V fatigue life.

Some specialized ASTM procedures for 3D-printed metal materials address the material properties expected for powder-based sintering implementations. Mechanical characteristics commonly reported include ultimate stress or maximum stress caused by stress, as well as elongation during breakage. The elastic modulus is calculated by dividing the stress by the strain. SLA materials are harder and more fragile than injection-molded counterparts are. They have such a different flexural and small elastic deformation before the dog's bone stress fractures as shown in Fig. 11.14 [133].

11.6.3 Compressive Test Properties of AM Developed Metal Components

The mechanical characteristics of metal AM components have also been evaluated using compressive testing. An investigation of the SLM-assembled tantalum amalgam found that the compressive yield strength was higher upward than evenly. The reason is that crystallographic surfaces are shifting. Despite its anisotropy stiffness, the mechanical properties of the SLM tantalum compound were found to be superior to those of an electron pillar heater or powder metallurgy. Basic design may be used to plan mechanical anisotropy in a segment [91]. During the investigation, anisotropic shifting level was observed in several cross-sectional schemes of EBM assemblies (Ti-6Al-4 V). The compressive force anisotropy was determined by the size of the cross-sectional structural unit. During compression tests in compression according to DIN 50,106, the specimens were continuously distorted until a predicted minimum height was reached [20].

The compressive elasticity module and the compressive output power R_{dp} have been calculated within the linear elasticity zone. The center of the exemplar was used to record deformation values in the specimen areas subject to uniaxial stress alone by means of a fine stretcher extensometer with a starting length of 1 cm. The compressive output strength is good at 75° and 90° (Fig. 11.15). Although porosity is a significant defect in SLM materials, it is recognized that it is only a vital factor in compressive loads. This is because, while the porosity is modest, the idea of heap shuts pores and produces flaws. Surprisingly, the pores expand, mix and distribute under folding stacking, leading to misleading [80]. When the results are checked, the influence of porosity on the direction of the stacking layer will most likely be determined. This would suggest that flaws have a wider impact when the direction of the layer corresponds to the stacking path and when the direction of the layer is animated along these lines than when the direction of the layer is reversed. The samples would have high compression yield strength at 75° and 90°. When compared

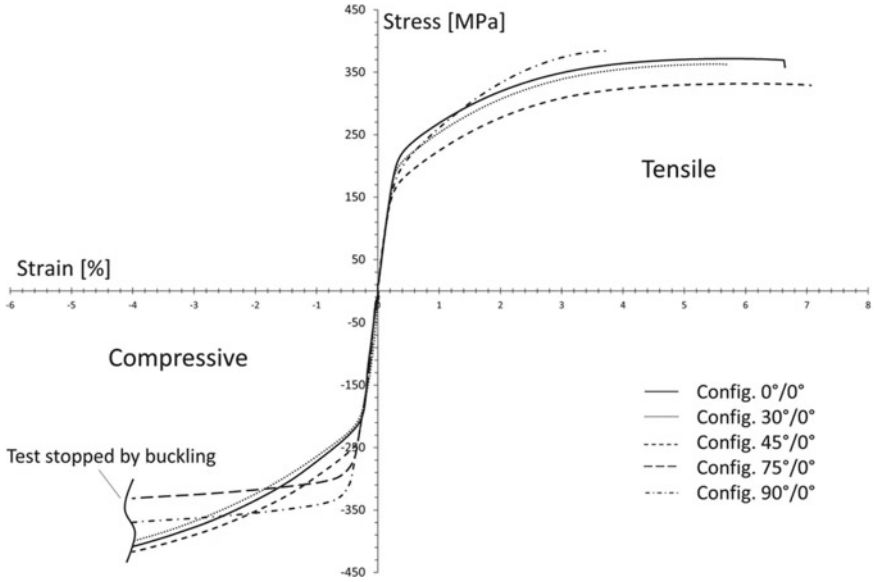
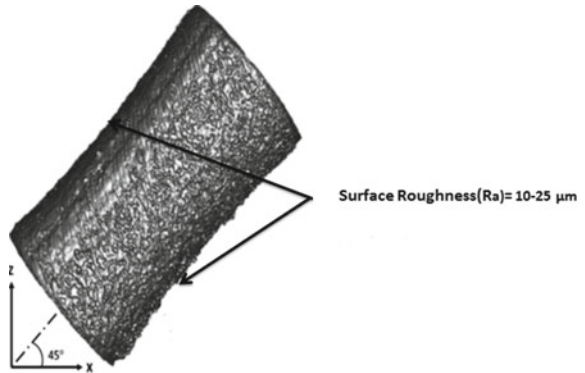


Fig. 11.15 Stress–strain curves compressive and tensile diagram [80]

Fig. 11.16 Demonstrating a larger surface roughness [101] (Down-Upward facing side)



to the results of the related study from [5], the results of the 90° cases indicate that the compressive yield strength is comparably inclined (Fig. 11.16).

11.6.4 Surface Roughness Properties of AM Developed Metal Components

A variety of inputs influences the surface characteristics of AM components, resulting in the development of various visible and quantifiable output variables that influence

performance. Input parameters include material presentation, component design, process sections, process parameters, and post-processing. Benefits range from partially fused powder granules (or beads) to improper melting because of construction, fusing, or detecting routes, such as balling Fig. 11.17a layer of fusion absence, or striation. The surface roughness of joint replacement bone interface implants, for example, may contribute to faster development, and thus periosteum—direct physical and functional contact between live tissue and the load-bearing implant surface—may be characterized as fastest and possibly most effective.

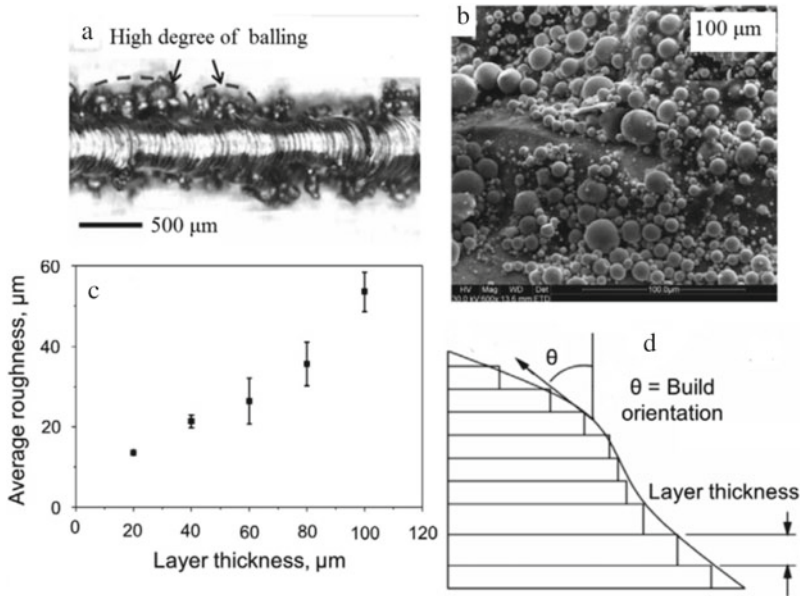


Fig. 11.17 a Balling effects [35] b solid granules on the construction surface [56] c surface roughness versus layer thickness [67] d surface roughness because of stairwell effects [66]

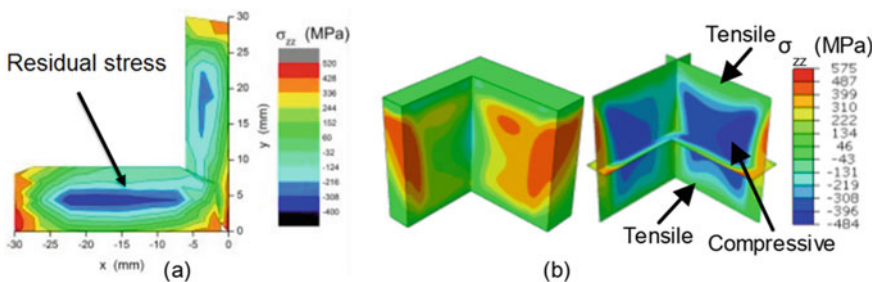


Fig. 11.18 Typical residual stress of an as-SLM item in the building direction a contours residual stress b anticipated residual stress

Surface roughness is one of the most detrimental effects on performing metal products and rotating fatigue. As a result, post-production activities are usually required to extend the life of AM components. This is difficult because many AM components, especially those with complicated geometry, want to be used as net-shaped as they were produced. As a result, after-surface treatment product loses one of AM's primary advantages: the ability to produce complex geometry that conventional manufacturing cannot [24]. Consequently, the fatigue of the components and their relationship to the surface coating must be fully known. The type of equipment used, powder size, process parameters, and orientation of the device can all affect the surface hardness of an AM surface. It is, thus, essential to fully understand fatigue. Because of the use of thicker hatches, DLD techniques typically produce the rough surfaces found in L-PBF techniques, due there is a lot of powder, pieces, and layers in this area. Increased hatching pitch, layer thickness, and/or powder size improve the surface hardness of AM components [105]. An X-ray CD image of a 45-degree Inconel 718 model created with the L-PBF method is shown here in Fig. 11.16. The excessive roughness on the face is caused by direct contact. Powder bedding is used throughout the manufacturing process, resulting in thermal decomposition pool heat/liquid fringe effects [101].

A mixture of many input parameters and processing situations determines surface hardness optimization and reduction. The type and procedure of the powder (10–60 μm powder), the powder circulation, and the material used for roller/blade spreading can all affect the hardness of the surface of the extremely low range of the PSD (Fig. 11.17c). The PBF-EB technique employs powder sizes ranging from 45 to 105 μm (Fig. 11.17b), which reduces the impact of electric charge, dissipation, powder flow ability, and diffusion disturbance on powder layer thickness (Fig. 11.17d). For example, transferring high PSDs to high surface hardness due to a process disruption results in an electrically charged PBF-EB surface that is slightly rich [75].

11.6.5 Fracture Toughness Properties of AM Developed Metal Components

The ability of a material to withstand fracture is described by its break strength. Based on various studies, Table 11.4 organizes the discovered crack strength benefits of specific metal AM components. Crack-life anisotropy was considered in both the SLM-assembled and EBM-assembled Ti-6Al-4 V. Because of break durability, anisotropy had an effect on how breaks spread.

Breaks occur across the columnar grains in evenly oriented examples, whereas breaks occur at the grain column boundaries in upwardly oriented examples [26]. The fracture force of EBM-built Ti-6Al-4 V is comparable to the specifications for Ti-6Al-4 V constructions or castings of 44–66 $\text{MPa m}^{1/2}$ and 88–110 $\text{MPa m}^{1/2}$, respectively. The reduced durability values reported in SLM-produced Ti-6Al-4 V are due to the

Table 11.4 Fracture toughness of different metallic materials are generated AM process

Process/Model	Material	Anisotropy in fracture toughness (%)	Fracture toughness (MPa \sqrt{m})	References
EBM/Arcam (A1)	Ti-6Al-4 V	7.3	110 \pm 7.4	Edwards [26]
EBM/Arcam (A2)	Ti-6Al-4 V	18.8	67–80	Seifi [77]
SLM	Ti-6Al-4 V	17.9	28 \pm 2	Cain [19]
LBM-MTT 250	Ti-6Al-4 V	3.1	66.9 \pm 2.6	Edwards [27]
SLM	Al-12Si	18.8	46.7	Suryawanshi [87]

fine acicular alpha/beta martensitic microstructure, which is more brittle than EBM-assembled Ti-6Al-4 V / duplex microstructure. Anisotropic break strength can result from residual stresses on metal AM components [19]. The use of post-warm therapy treatments may minimize residual stresses such as HIP or stress reduction treatment. Following SLM-built Ti-6Al-4 V therapy with HIP and stress relief, fracture strength improved and anisotropy reduced, according to research utilizing SLM Ti-6Al-4 V. In any case, a review on EBM-constructed Ti-6Al-4 V demonstrated a decrease in break strength after heat treatment procedures, which came from microstructure coarsening. Understandings of the as-built microstructures for the unique metal AM frameworks are critical in determining post-heat treatment approaches to provide superior fracture durability [19, 87].

11.6.6 Fatigue Strength in AM Metal

The fatigue strength of such metals is determined by the static mechanical properties of materials that are identical to the microstructure of various metals. However, the fatigue performance of AM-produced parts is poor because of inherent properties, such as surface ruggedness and material failures. AM process is used to conduct experiments for the study of monotonic tensile behavior of different metals and alloys. The wear-out characteristics of the additive Ti-6Al-4 V have been investigated (Table 11.5) because of its potential use in aviation and biomedical applications [7, 100]. Comparing the fatigue characteristics of PBF-EB and DMLS made from Ti-6Al-4 V, the lower the wear rate, the better the fatigue strength of both was found (DMLS reached 107 cycles at 550–600 MPa, EBM at 600 MPa as shown in Table 11.5). Surface modifications can help improve fatigue properties (e.g. polishing). Brandl et al. [14] the scatter of investigative data increases material failures, such as porosity and lack of adhesion on the layer, making tribological characteristics difficult to evaluate.

Using hot isostatic pressings to cure and density these defects results in higher wear-out and real data, similar to AM processes. Table 11.5 summarizes the fatigue

Table 11.5 Fatigue strength of different metallic materials are generated AM process

Am techniques	Materials	Referenced by	Surface treatment	Condition Kelvin /Celsius	σ Smax at 107 [MPa]
EBM	Ti-6Al-4 V	Brandl et al. [14]	Refined	843 C/100 MPa/4 h-HIP	600
LMD	Ti-6Al-4 V	Brandl et al. [14]	Refined	ST-843 C/2 h	-700
LBM	Ti-6Al-4 V	Leuders et al. [47]	Not mentioned	920 C/100 MPa/ 2 h-HIP	620
LBM	AlSi ₁₂	Siddique et al. [81]	Refined	473.15 K in process b SR-240 C/6 h	80
LBM	AlSi ₁₀ Mg	Buchbinder et al. [17]	Refined	AF	45
LBM	AlMg _{4.4} Sc _{0.66} MnZ	Buchbinder et al. [17]	Refined	AA-325 C/4 h	300
LBM	316L	Riemer et al. [71]	Precision-machined	HIP-1150 C/100 MPa/4 h	317

ST Solution Treated, AF Manufacturing, SR Stress Relieved

strength got through the different surface and thermal treating conditions of AM-based metals such as aluminum alloys, Ti-6Al-4 V, and steels. The study shows that AM raw materials are comparable to standard products, such as static and fatigue strength, in terms of their physical fragmentation and mechanical properties, and that mechanical behavioral concepts can be used for the analysis of AM metals and alloys [33, 71].

11.6.7 Creep in AM Metals

Variability in the creeping properties of fatigue-related components in both AM and conventional components indicates failures as well as an improvement in the fine microstructure. Because of the complexities of creep tests, such as thermal processing ranges, stress and pressure, temperature measurement, and the scarcity of research, no consistent trends in the creeps of additively manufactured metals can be identified. Creep-Fracture of IN 738LC, and added into high corrosion resistance precipitation-enforced created through PBF-L, has already been discovered to be anisotropic. The inhomogeneity of the minimal column grain was created in part by its solid texture as an anisotropic elastic strap [70]. A detailed study on CCM composites (Co-28Cr-6Mo-0.23C-0.17 N) manufactured using Powder Bed Fusion Electron Beam (PBF-EB) process was conducted by Sun [85]. This CCM composite is made up of crystalline structure columnar morphology c-Fcc

and stabilized equiaxed morphology (e-hcp) phases in its as-built state. To prevent transformation during experiments, the substance was dramatically changed to e-hcp before cramping. Because the PBF-EB technique keeps the building chamber at a higher temperature (700 C), the granules near the center plate continue to grow longer than those near the top [86]. In that, E-grains were discovered to be larger in the as-produced lower part of the components than after heat treatment processing. The results show that the grain-boundary mechanism for flexibility creep promotes the formation and distribution of voids across the grain bounds. A two-step thermal process reflecting the temperature history in the PBF-EB method was proposed [47, 81], to increase grained area through buildings while ignoring grain failure zones.

11.6.8 Analysis of Residual Stress in AM Developed Metal Parts

Scanner methods, dwell time, and a variety of other factors all have an impact on the residual stress field of metal AM components. Previous heat transfer parameters have a significant impact. The residual surface stress of an SLM treated steel 316 L-shaped bar (off foot molecule) was studied using a digital picture contact mode and neutron differentiation, according to Ahmad et al. Compression and traction near surfaces, as well as residual stress near the area's centre, are depicted in Fig. 11.18a. The effects of the scanning method, laser energy scanning velocity, and residual stress orientation are all investigated thoroughly [7]. Lesyk et al. [46] investigated the effect of island size on residual stress and discovered a similar pattern. Even though the size of the island was shown to result in low residual stress of $2 \times 2 \text{ mm}^2$, significant fractures were discovered in the model created with this island size. As shown in (Fig. 18b), this pattern was captured by modeling and experimental research with an important residual stress forecast in the DED-treated Vaseline zone.

Evaluation of residual stress using SLM X-ray diffraction Xiao et al. [100] discovered that residual stress in the scanning trajectory is greatest at a higher tensile and constructed interface than in the perpendicular motion using small-scale models of treated steel and Ti6Al4V. Kruth et al. [44] devised a method for calculating the residual stress of the SLM segment based on bridge curvature. Other researchers developed a method for determining residual stress in SLM components quickly. The amount of residual stress in the bridge-formed component after it's removed from the foundation is determined by the curved tilt of the structure's two-base surfaces. Framework variables such as scan vector distance and scan scalar rotation grades were investigated for two consecutive layers, and it was discovered that controlling rest stress and displacement during the SLM technique necessitates a shorter scan vector length and a greater revolution inclination.

The residual stress of EBM processed elements is noticeably lower than that of SLM processed elements because the cooling fee is based on the resulting solidification capabilities of those methods, such as protoplasmic processes arm spacing. The

cooling rate in the EBM is significantly lower, and energy drainage from the EBM component takes longer, because of the Pulver surface and vacuum container being highly post-heated [45, 131]. Salem et al. [73] used nuclear diffraction to investigate the residual stress of Inconel 718 cubes treated with EBM and SLM in their as-built state. The researchers used (Electric Discharge Machining-EDM) to create stress-free samples to determine pressure-remote network spacing. Because SLM is further from homeostasis than EBM, every residual stress element generated by EBM reduces the order value of SLM.

The residual stress of SS 316L and Inconel 718 additives made with DEDs via nuclear crystallography and contour approach was investigated/ [60] the remaining stress within the sample centers was caused by uniaxial compaction. Longitudinal residual stress was detected at the edges and was found to be related to the construction method. Residual stress magnitudes in the cloth were greater than 50–60% of the nominal output electricity [49]. The effects of dwell time on residue stress and deformations in DED-processed Ti64 and Inconel 625 systems were investigated. The well-known Inconel 625 structure exhibits the inverse trend, resulting in significantly less residual stress during the deposition phase. Reducing the refresh time for Ti64 builds can result in significantly lower residual stress as the DED process progresses.

11.7 Conclusions

A detailed investigation of the status of metal additive manufacturing, with astonishing connections between process parameters, mechanical properties and metals has been carried out. According to the Hall-Patch regulation, “High sturdiness AM inclination creates fine-grain microstructures”. Unbalanced micro-sized structures, such as austenite, titanium, or titanium-based alloys with a martensite alpha phase, are exposed as a result of materials and manufacturing techniques. AM processes contain anisotropic microstructures with elongated grain due to anisotropic thermal conductivity, and the formation process in current structural layers is significant, resulting in the development of non-directional properties. Typically, reheating and treating solidified layers on the ground are part of the complicated AM’s temperature cycle. This could result in both desired and unintended consequences, such as a breakdown in ductile varieties, alloy component partitioning, and grain growth. Further ex-situ thermal processing can alter the microstructure and characteristics of the final component in different methods. In the process of fabricating the metal components, which affected its final structure and mechanical characteristics, it was subjected to preparation elements such as declaration rate, pillar power, climate and temperature. The mechanical properties of metal AM components (e.g., durability and rigidity) can frequently meet its basic needs through comparison of cast and model equivalents despite anisotropy and variability.

Integrating a diverse set of input components and processing scenarios aids in the optimization and reduction of surface roughness. Welding terms such as loss

of sidewall fusion, undercutting, an anomalous pinnacle bead, and an increase in craters are used to describe surface roughness. The words for entering data in twine-driven systems are similar. This occurs on a much larger scale because of the large diameters of the molded pools, deposit bead widths, and later heights. In segment 5.4, the PBF-EB technique employs particle sizes ranging from 45 to 125 μm to reduce the effects of electrostatic transport. The EBM-manufactured Ti-6Al-4 V was shown to be dependent on the area in terms of durability of a crack due to microstructure and defect dispersion. Although the mechanical properties of metal AM components are anisotropic and heterogeneous, they are assumed to have the same or superior mechanical qualities as casted components.

The purpose of Sect. 5.7 is to summarize residual strain in AM metal. An excessive increase and rapid cooling exacerbate the residual strain. Pre-heating, approach training, remark strategic planning, and laser annealing are all individual methods for reducing long-term pressure. The presence of a substructure has a significant impact on the magnitude of residual stresses. According to the findings, the metallic AM processing and heating treatments are precise stress-discount strategies. Many statistics on fatigue and fracture toughness properties, as well as tensile and compressive properties, were calculated. According to the literature, various categories of steel, aluminum composites, and titanium materials designed and produced by LMD, LBM, and EBM have typical properties equivalent to cast or wrought processes. Most existing applications and innovation demonstration models are limited to non-existent or insignificant components in the face of variable loads. Recent studies on the efficacy of fatigue are about to change this. As a result, a sequential approach to AM can be used for a wide range of material process combinations.

11.8 Future Trends

AM can be used to create complex components such as jewels, dental implants, and electrical wires out of valuable metals such as gold, silver, palladium, and platinum. AM has distinct advantages for producing components of high liquefying conditioned inert composite materials, which are in high demand when manufactured using traditional methods. Powder-based AM methods have only recently become available. It is also used to improve the texture and properties of products by combining them in various ways. The research focused on the development of high-tech materials such as tantalum, molybdenum, chromium, tungsten, rhenium, niobium, and vanadium, which had unrivalled potential for future generation AM.

References

1. Abd-Elghany, K., Bourell, D.L.: Property evaluation of 304L stainless steel fabricated by selective laser melting. *Rapid Prototyp. J.* **18**, 420–428 (2012). <https://doi.org/10.1108/135>

- 52541211250418
2. Aboulkhair, N.: Additive manufacture of an aluminium alloy: processing, microstructure, and mechanical properties, (2015)
 3. Aboulkhair, N.T., Maskery, I., Tuck, C., Ashcroft, I., Everitt, N.M.: The microstructure and mechanical properties of selectively laser melted AlSi₁₀Mg: the effect of a conventional T6-like heat treatment. *Mater. Sci. Eng. A* **667**, 139–146 (2016). <https://doi.org/10.1016/j.msea.2016.04.092>
 4. Aboulkhair, N.T., Simonelli, M., Parry, L., Ashcroft, I., Tuck, C., Hague, R.: 3D printing of aluminium alloys: additive manufacturing of aluminium alloys using selective laser melting. *Prog. Mater. Sci.* **106**, 100578 (2019). <https://doi.org/10.1016/j.pmatsci.2019.100578>
 5. Aboulkhair, N.T., Tuck, C., Ashcroft, I., Maskery, I., Everitt, N.M.: On the precipitation hardening of selective laser melted AlSi₁₀Mg. *Metall Mater Trans A*. **46**, 3337–3341 (2015). <https://doi.org/10.1007/s11661-015-2980-7>
 6. Ahangar, P., Cooke, M.E., Weber, M.H., Rosenzweig, D.H.: Current biomedical applications of 3D printing and additive manufacturing. *Appl. Sci.* **9**, 1713 (2019). <https://doi.org/10.3390/app9081713>
 7. Ahmad, B., van der Veen, S.O., Fitzpatrick, M.E., Guo, H.: Residual stress evaluation in selective-laser-melting additively manufactured titanium (Ti-6Al-4V) and inconel 718 using the contour method and numerical simulation. *Addit. Manuf.* **22**, 571–582 (2018). <https://doi.org/10.1016/j.addma.2018.06.002>
 8. Ahn, D.-G.: Direct metal additive manufacturing processes and their sustainable applications for green technology: a review. *Int. J. Precis. Eng. Manuf. Green Tech.* **3**, 381–395 (2016). <https://doi.org/10.1007/s40684-016-0048-9>
 9. Ambrogio, G., Gagliardi, F., Bruschi, S., Filice, L.: On the high-speed single point incremental forming of titanium alloys. *CIRP Ann.* **62**, 243–246 (2013). <https://doi.org/10.1016/j.cirp.2013.03.053>
 10. Bai, Y., Yang, Y., Wang, D., Zhang, M.: Influence mechanism of parameters process and mechanical properties evolution mechanism of maraging steel 300 by selective laser melting. *Mater. Sci. Eng. A* **703**, 116–123 (2017). <https://doi.org/10.1016/j.msea.2017.06.033>
 11. Bian, L., Thompson, S.M., Shamsaei, N.: Mechanical properties and microstructural features of direct laser-deposited Ti-6Al-4V. *JOM.* **67**, 629–638 (2015). <https://doi.org/10.1007/s11837-015-1308-9>
 12. Blackwell, P.L.: The mechanical and microstructural characteristics of laser-deposited IN718. *J. Mater. Process. Technol.* **170**, 240–246 (2005). <https://doi.org/10.1016/j.jmatprotec.2005.05.005>
 13. Bobbio, L., Qin, S., Dunbar, A., Michaleris, P., Beese, A.: Characterization of the strength of support structures used in powder bed fusion additive manufacturing of Ti-6Al-4V. *Addit. Manuf.* **14**, (2017). <https://doi.org/10.1016/j.addma.2017.01.002>
 14. Brandl, E., Palm, F., Michailov, V., Viehweger, B., Leyens, C.: Mechanical properties of additive manufactured titanium (Ti-6Al-4V) blocks deposited by a solid-state laser and wire. *Mater. Des.* **32**, 4665–4675 (2011). <https://doi.org/10.1016/j.matdes.2011.06.062>
 15. Bresser, D., Hosoi, K., Howell, D., Li, H., Zeisel, H., Amine, K., Passerini, S.: Perspectives of automotive battery R&D in China, Germany, Japan, and the USA. *J. Power Sources* **382**, 176–178 (2018). <https://doi.org/10.1016/j.jpowsour.2018.02.039>
 16. Brice, C., Shenoy, R., Kral, M., Buchannan, K.: Precipitation behavior of aluminum alloy 2139 fabricated using additive manufacturing. *Mater. Sci. Eng. A* **648**, 9–14 (2015). <https://doi.org/10.1016/j.msea.2015.08.088>
 17. Buchbinder, D., Meiners, W., Pirch, N., Wissenbach, K., Schrage, J.: Investigation on reducing distortion by preheating during manufacture of aluminum components using selective laser melting. *J. Laser Appl.* **26**, 012004 (2014). <https://doi.org/10.2351/1.4828755>
 18. Caba, S.: Aluminum alloy for additive manufacturing in automotive production. *ATZ Worldw.* **122**, 58–61 (2020). <https://doi.org/10.1007/s38311-020-0285-y>
 19. Cain, V., Thijs, L., Van Humbeeck, J., Van Hooreweder, B., Knutsen, R.: Crack propagation and fracture toughness of Ti₆Al₄V alloy produced by selective laser melting. *Addit. Manuf.* **5**, 68–76 (2015). <https://doi.org/10.1016/j.addma.2014.12.006>

20. Cansizoglu, O., Harrysson, O., Cormier, D., West, H., Mahale, T.: Properties of Ti-6Al-4V non-stochastic lattice structures fabricated via electron beam melting. *Mater. Sci. Eng. A* **492**, 468–474 (2008). <https://doi.org/10.1016/j.msea.2008.04.002>
21. Carlton, H.D., Haboub, A., Gallegos, G.F., Parkinson, D.Y., MacDowell, A.A.: Damage evolution and failure mechanisms in additively manufactured stainless steel. *Mater. Sci. Eng., A* **651**, 406–414 (2016). <https://doi.org/10.1016/j.msea.2015.10.073>
22. Chan, K.S., Koike, M., Mason, R.L., Okabe, T.: Fatigue life of titanium alloys fabricated by additive layer manufacturing techniques for dental implants. *Metall Mater Trans A* **44**, 1010–1022 (2013). <https://doi.org/10.1007/s11661-012-1470-4>
23. DebRoy, T., Wei, H.L., Zuback, J.S., Mukherjee, T., Elmer, J.W., Milewski, J.O., Beese, A.M., Wilson-Heid, A., De, A., Zhang, W.: Additive manufacturing of metallic components—process, structure and properties. *Prog. Mater. Sci.* **92**, 112–224 (2018). <https://doi.org/10.1016/j.pmatsci.2017.10.001>
24. Doornewaard, R., Christiaens, V., Bruyn, H.D., Jacobsson, M., Cosyn, J., Vervaeke, S., Jacquet, W.: Long-Term effect of surface roughness and patients’ factors on crestal bone loss at dental implants. A systematic review and meta-analysis. *Clin. Implant Dent. Relat Res.* **19**, 372–399 (2017). <https://doi.org/10.1111/cid.12457>
25. Dutta, B., Froes, F.H.: (Sam): The additive manufacturing (AM) of titanium alloys. *Met. Powder Rep.* **72**, 96–106 (2017). <https://doi.org/10.1016/j.mprp.2016.12.062>
26. Edwards, P., O’Conner, A., Ramulu, M.: Electron beam additive manufacturing of titanium components: properties and performance. *J. Manuf. Sci. Eng.* **135**, (2013). <https://doi.org/10.1115/1.4025773>
27. Edwards, P., Ramulu, M.: Effect of build direction on the fracture toughness and fatigue crack growth in selective laser melted Ti-6Al-4 V. *Fatigue Fract. Eng. Mater. Struct.* **38**, 1228–1236 (2015). <https://doi.org/10.1111/ffe.12303>
28. Frazier, W.E.: Metal additive manufacturing: a review. *J. Mater Eng Perform.* **23**, 1917–1928 (2014). <https://doi.org/10.1007/s11665-014-0958-z>
29. Fulcher, B.A., Leigh, D.K., Watt, T.J.: Comparison of AlSi₁₀Mg and Al 6061 processed through DMLS. **16**
30. Galati, M.: Chapter 8—Electron beam melting process: a general overview. In: Pou, J., Riveiro, A., and Davim, J.P. (eds.) *Additive Manufacturing*, pp. 277–301. Elsevier (2021)
31. Gorse, S., Hutchinson, C., Gouné, M., Banerjee, R.: Additive manufacturing of metals: a brief review of the characteristic microstructures and properties of steels, Ti-6Al-4V and high-entropy alloys. *Sci. Technol. Adv. Mater.* **18**, 584–610 (2017). <https://doi.org/10.1080/14686996.2017.1361305>
32. Graf, B., Schuch, M., Petrat, T., Gumenyuk, A., Rethmeier, M.: Combined laser additive manufacturing with powderbed and powder nozzle for turbine parts. In: Presented at the Proceedings of 6th International Conference and Additive Technologies (2016)
33. Greitemeier, D., Palm, F., Syassen, F., Melz, T.: Fatigue performance of additive manufactured TiAl₆V₄ using electron and laser beam melting. *Int. J. Fatigue* **94**, 211–217 (2017). <https://doi.org/10.1016/j.ijfatigue.2016.05.001>
34. Gu, D.: Materials creation adds new dimensions to 3D printing. *Sci. Bull.* **61**, 1718–1722 (2016). <https://doi.org/10.1007/s11434-016-1191-y>
35. Gu, D., Shen, Y.: Balling phenomena in direct laser sintering of stainless steel powder: metallurgical mechanisms and control methods. *Mater. Des.* **30**, 2903–2910 (2009). <https://doi.org/10.1016/j.matdes.2009.01.013>
36. Haghdadi, N., Laleh, M., Moyle, M., Primig, S.: Additive manufacturing of steels: a review of achievements and challenges. *J Mater Sci.* **56**, 64–107 (2021). <https://doi.org/10.1007/s10853-020-05109-0>
37. Herzog, D., Seyda, V., Wycisk, E., Emmelmann, C.: Additive manufacturing of metals. *Acta Mater.* **117**, 371–392 (2016). <https://doi.org/10.1016/j.actamat.2016.07.019>
38. Hinojos, A., Mireles, J., Reichardt, A., Frigola, P., Hosemann, P., Murr, L.E., Wicker, R.B.: Joining of inconel 718 and 316 stainless steel using electron beam melting additive manufacturing technology. *Mater. Des.* **94**, 17–27 (2016). <https://doi.org/10.1016/j.matdes.2016.01.041>

39. Hrabe, N., Quinn, T.: Effects of processing on microstructure and mechanical properties of a titanium alloy (Ti–6Al–4V) fabricated using electron beam melting (EBM), Part 2: Energy input, orientation, and location. *Mater. Sci. Eng., A* **573**, 271–277 (2013). <https://doi.org/10.1016/j.msea.2013.02.065>
40. Hunt, J.D.: Steady state columnar and equiaxed growth of dendrites and eutectic. *Mater. Sci. Eng.* **65**, 75–83 (1984). [https://doi.org/10.1016/0025-5416\(84\)90201-5](https://doi.org/10.1016/0025-5416(84)90201-5)
41. Kannan, G.B., Rajendran, D.K.: A review on status of research in metal additive manufacturing. *Adv. 3D Print. Addit. Manuf. Technol.*, 95–100 (2017). https://doi.org/10.1007/978-981-10-0812-2_8
42. Kasperovich, G., Hausmann, J.: Improvement of fatigue resistance and ductility of TiAl₆V₄ processed by selective laser melting. *J. Mater. Process. Technol.* **220**, 202–214 (2015). <https://doi.org/10.1016/j.jmatprotec.2015.01.025>
43. Ko, G., Kim, W., Kwon, K., Lee, T.-K.: The corrosion of stainless steel made by additive manufacturing: a review. *Metals*. **11**, 516 (2021). <https://doi.org/10.3390/met11030516>
44. Kruth, J., Mercelis, P., Van Vaerenbergh, J., Froyen, L., Rombouts, M.: Binding mechanisms in selective laser sintering and selective laser melting. *Rapid Prototyp J.* **11**, 26–36 (2005). <https://doi.org/10.1108/13552540510573365>
45. Kundakcioglu, E., Lazoglu, I., Poyraz, Ö., Yasa, E., Cizicioglu, N.: Thermal and molten pool model in selective laser melting process of Inconel 625. *Int J Adv Manuf Technol.* **95**, 3977–3984 (2018). <https://doi.org/10.1007/s00170-017-1489-1>
46. Lesyk, D.A., Martinez, S., Mordiyuk, B.N., Dzhemelinskyi, V.V., Lamikiz, A., Prokopenko, G.I.: Post-processing of the Inconel 718 alloy parts fabricated by selective laser melting: effects of mechanical surface treatments on surface topography, porosity, hardness and residual stress. *Surf. Coat. Technol.* **381**, 125136 (2020). <https://doi.org/10.1016/j.surfcoat.2019.125136>
47. Leuders, S., Thöne, M., Riemer, A., Niendorf, T., Tröster, T., Richard, H.A., Maier, H.J.: On the mechanical behaviour of titanium alloy TiAl₆V₄ manufactured by selective laser melting: fatigue resistance and crack growth performance. *Int. J. Fatigue* **48**, 300–307 (2013). <https://doi.org/10.1016/j.ijfatigue.2012.11.011>
48. Lewandowski, J.J., Seifi, M.: Metal additive manufacturing: a review of mechanical properties. *Annu. Rev. Mater. Res.* **46**, 151–186 (2016). <https://doi.org/10.1146/annurev-matsci-070115-032024>
49. Li, C., Liu, Z.Y., Fang, X.Y., Guo, Y.B.: Residual stress in metal additive manufacturing. *Procedia CIRP*. **71**, 348–353 (2018). <https://doi.org/10.1016/j.procir.2018.05.039>
50. Martinez, E., Murr, L.E., Amato, K.N., Hernandez, J., Shindo, P.W., Gaytan, S.M., Ramirez, D.A., Medina, F., Wicker, R.B.: 3D microstructural architectures for metal and alloy components fabricated by 3D printing/additive manufacturing technologies. In: De Graef, M., Poulsen, H.F., Lewis, A., Simmons, J., and Spanos, G. (eds.) *Proceedings of the 1st International Conference on 3D Materials Science*, pp. 73–78. Springer International Publishing, Cham (2016)
51. Mehta, A., Zhou, L., Huynh, T., Park, S., Hyer, H., Song, S., Bai, Y., Imholte, D.D., Woolstenhulme, N.E., Wachs, D.M., Sohn, Y.: Additive manufacturing and mechanical properties of the dense and crack free Zr-modified aluminum alloy 6061 fabricated by the laser-powder bed fusion. *Addit. Manuf.* **41**, 101966 (2021). <https://doi.org/10.1016/j.addma.2021.101966>
52. Mirzababaei, S., Pasebani, S.: A review on binder jet additive manufacturing of 316L stainless steel. *J. Manuf. Mater. Process.* **3**, 82 (2019). <https://doi.org/10.3390/jmmp3030082>
53. Monteiro, W.A.: *Light Metal Alloys Applications*. BoD—Books on Demand (2014)
54. Monzón, M.D., Ortega, Z., Martínez, A., Ortega, F.: Standardization in additive manufacturing: activities carried out by international organizations and projects. *Int J Adv Manuf Technol.* **76**, 1111–1121 (2015). <https://doi.org/10.1007/s00170-014-6334-1>
55. Morrow, B.M., Lienert, T.J., Knapp, C.M., Sutton, J.O., Brand, M.J., Pacheco, R.M., Livescu, V., Carpenter, J.S., Gray, G.T.: Impact of defects in powder feedstock materials on microstructure of 304L and 316L stainless steel produced by additive manufacturing. *Metall Mat Trans A.* **49**, 3637–3650 (2018). <https://doi.org/10.1007/s11661-018-4661-9>

56. Mumtaz, K., Hopkinson, N.: Top surface and side roughness of Inconel 625 parts processed using selective laser melting. *Rapid Prototyp. J.* **15**, 96–103 (2009). <https://doi.org/10.1108/13552540910943397>
57. Murr, L.E.: Metallurgy of additive manufacturing: examples from electron beam melting. *Addit. Manuf.* **5**, 40–53 (2015). <https://doi.org/10.1016/j.addma.2014.12.002>
58. Ngo, T.D., Kashani, A., Imbalzano, G., Nguyen, K.T.Q., Hui, D.: Additive manufacturing (3D printing): a review of materials, methods, applications and challenges. *Compos. B Eng.* **143**, 172–196 (2018). <https://doi.org/10.1016/j.compositesb.2018.02.012>
59. Patterson, A.E., Messimer, S.L., Farrington, P.A.: Overhanging features and the SLM/DMLS residual stresses problem: review and future research need. *Technologies.* **5**, 15 (2017). <https://doi.org/10.3390/technologies5020015>
60. Phan, T.Q., Strantzla, M., Hill, M.R., Gnapel-Herold, T.H., Heigel, J., D’Elia, C.R., DeWald, A.T., Clausen, B., Pagan, D.C., Peter Ko, J.Y., Brown, D.W., Levine, L.E.: Elastic residual strain and stress measurements and corresponding part deflections of 3D additive manufacturing builds of IN625 AM-bench artifacts using neutron diffraction, synchrotron X-Ray diffraction, and contour method. *Integr Mater Manuf Innov.* **8**, 318–334 (2019). <https://doi.org/10.1007/s40192-019-00149-0>
61. Pollack, S., Venkatesh, C., Neff, M., Healy, A.V., Hu, G., Fuenmayor, E.A., Lyons, J.G., Major, I., Devine, D.M.: Polymer-Based additive manufacturing: historical developments, process types and material considerations. In: Devine, D.M. (ed.) *Polymer-Based Additive Manufacturing: Biomedical Applications*, pp. 1–22. Springer International Publishing, Cham (2019)
62. Popov, V.V., Fleisher, A.: Hybrid additive manufacturing of steels and alloys. *Manuf. Rev.* **7**, 6 (2020). <https://doi.org/10.1051/mfreview/2020005>
63. Prakash, K.S., Nancharaih, T., Rao, V.V.S.: Additive manufacturing techniques in manufacturing—an overview. *Materials Today: Proceedings.* **5**, 3873–3882 (2018). <https://doi.org/10.1016/j.matpr.2017.11.642>
64. Prashanth, K.G., Scudino, S., Klauss, H.J., Surreddi, K.B., Löber, L., Wang, Z., Chaubey, A.K., Kühn, U., Eckert, J.: Microstructure and mechanical properties of Al–12Si produced by selective laser melting: effect of heat treatment. *Mater. Sci. Eng. A* **590**, 153–160 (2014). <https://doi.org/10.1016/j.msea.2013.10.023>
65. Qiu, C., Adkins, N.J.E., Attallah, M.M.: Microstructure and tensile properties of selectively laser-melted and of HIPed laser-melted Ti-6Al-4V. *Mater. Sci. Eng. A* **578**, 230–239 (2013). <https://doi.org/10.1016/j.msea.2013.04.099>
66. Qiu, C., Panwisawas, C., Ward, M., Basoalto, H.C., Brooks, J.W., Attallah, M.M.: On the role of melt flow into the surface structure and porosity development during selective laser melting. *Acta Mater.* **96**, 72–79 (2015). <https://doi.org/10.1016/j.actamat.2015.06.004>
67. Rahmati, S., Vahabli, E.: Evaluation of analytical modeling for improvement of surface roughness of FDM test part using measurement results. *Int J Adv Manuf Technol.* **79**, 823–829 (2015). <https://doi.org/10.1007/s00170-015-6879-7>
68. Reeves, P., Tuck, C., Hague, R.: Additive manufacturing for mass customization. In: Fogliatto, F.S., da Silveira, G.J.C. (eds.) *Mass Customization: Engineering and Managing Global Operations*, pp. 275–289. Springer, London (2011)
69. Revilla-León, M., Ceballos, L., Martínez-Klemm, I., Özcan, M.: Discrepancy of complete-arch titanium frameworks manufactured using selective laser melting and electron beam melting additive manufacturing technologies. *J. Prosthet. Dent.* **120**, 942–947 (2018). <https://doi.org/10.1016/j.prosdent.2018.02.010>
70. Rickenbacher, L., Etter, T., Hövel, S., Wegener, K.: High temperature material properties of IN738LC processed by selective laser melting (SLM) technology. *Rapid Prototyp. J.* **19**, 282–290 (2013). <https://doi.org/10.1108/13552541311323281>
71. Riemer, A., Leuders, S., Thöne, M., Richard, H.A., Tröster, T., Niendorf, T.: On the fatigue crack growth behavior in 316L stainless steel manufactured by selective laser melting. *Eng. Fract. Mech.* **120**, 15–25 (2014). <https://doi.org/10.1016/j.engfracmech.2014.03.008>

72. Saeidi, K., Zapata, D.L., Lofaj, F., Kvetkova, L., Olsen, J., Shen, Z., Akhtar, F.: Ultra-high strength martensitic 420 stainless steel with high ductility. *Addit. Manuf.* **29**, 100803 (2019). <https://doi.org/10.1016/j.addma.2019.100803>
73. Salem, M., Le Roux, S., Hor, A., Dour, G.: A new insight on the analysis of residual stresses related distortions in selective laser melting of Ti-6Al-4V using the improved bridge curvature method. *Addit. Manuf.* **36**, 101586 (2020). <https://doi.org/10.1016/j.addma.2020.101586>
74. Sames, W.J., Unocic, K.A., Dehoff, R.R., Lolla, T., Babu, S.S.: Thermal effects on microstructural heterogeneity of Inconel 718 materials fabricated by electron beam melting. *J. Mater. Res.* **29**, 1920–1930 (2014). <https://doi.org/10.1557/jmr.2014.140>
75. Schmidtke, K., Palm, F., Hawkins, A., Emmelmann, C.: Process and Mechanical Properties: applicability of a scandium modified Al-alloy for laser additive manufacturing. *Phys. Procedia* **12**, 369–374 (2011). <https://doi.org/10.1016/j.phpro.2011.03.047>
76. Scott, J., Gupta, N., Weber, C., Newsome, S., Wohlers, T., Associates, W., Caffrey, T., Associates, W.: *Additive Manufacturing: Status and Opportunities*. 36
77. Seifi, M., Dahar, M., Aman, R., Harrysson, O., Beuth, J., Lewandowski, J.J.: Evaluation of orientation dependence of fracture toughness and fatigue crack propagation behavior of as-deposited ARCAM EBM Ti-6Al-4V. *JOM.* **67**, 597–607 (2015). <https://doi.org/10.1007/s11837-015-1298-7>
78. Seifi, M., Salem, A., Beuth, J., Harrysson, O., Lewandowski, J.J.: Overview of materials qualification needs for metal additive manufacturing. *JOM.* **68**, 747–764 (2016). <https://doi.org/10.1007/s11837-015-1810-0>
79. Selcuk, C.: Laser metal deposition for powder metallurgy parts. *Powder Metall.* **54**, 94–99 (2011). <https://doi.org/10.1179/174329011X12977874589924>
80. Sert, E., Hitzler, L., Hafenstein, S., Merkel, M., Werner, E., Öchsner, A.: Tensile and compressive behaviour of additively manufactured AlSi₁₀Mg samples. *Prog Addit Manuf.* **5**, 305–313 (2020). <https://doi.org/10.1007/s40964-020-00131-9>
81. Siddique, S., Imran, M., Wycisk, E., Emmelmann, C., Walther, F.: Influence of process-induced microstructure and imperfections on mechanical properties of AlSi₁₂ processed by selective laser melting. *J. Mater. Process. Technol.* **221**, 205–213 (2015). <https://doi.org/10.1016/j.jmatprotec.2015.02.023>
82. Slotwinski, J., Moylan, S.: Applicability of existing materials testing standards for additive manufacturing materials. 17, (2014)
83. Spears, T.G., Gold, S.A.: In-process sensing in selective laser melting (SLM) additive manufacturing. *Integr Mater Manuf Innov.* **5**, 16–40 (2016). <https://doi.org/10.1186/s40192-016-0045-4>
84. Suave, L.M., Bertheau, D., Cormier, J., Villechaise, P., Soula, A., Hervier, Z., Laigo, J.: Impact of microstructural evolutions during thermal aging of Alloy 625 on its monotonic mechanical properties. *MATEC Web of Conferences.* **14**, 21001 (2014). <https://doi.org/10.1051/mateconf/20141421001>
85. Sun, S.-H., Koizumi, Y., Kurosu, S., Li, Y.-P., Chiba, A.: Phase and grain size inhomogeneity and their influences on creep behavior of Co–Cr–Mo alloy additive manufactured by electron beam melting. *Acta Mater.* **86**, 305–318 (2015). <https://doi.org/10.1016/j.actamat.2014.11.012>
86. Sun, S.-H., Koizumi, Y., Kurosu, S., Li, Y.-P., Matsumoto, H., Chiba, A.: Build direction dependence of microstructure and high-temperature tensile property of Co–Cr–Mo alloy fabricated by electron beam melting. *Acta Mater.* **64**, 154–168 (2014). <https://doi.org/10.1016/j.actamat.2013.10.017>
87. Suryawanshi, J., Prashanth, K.G., Scudino, S., Eckert, J., Prakash, O., Ramamurty, U.: Simultaneous enhancements of strength and toughness in an Al-12Si alloy synthesized using selective laser melting. *Acta Mater.* **115**, 285–294 (2016). <https://doi.org/10.1016/j.actamat.2016.06.009>
88. Tan, X., Kok, Y., Tan, Y.J., Descoins, M., Mangelinck, D., Tor, S.B., Leong, K.F., Chua, C.K.: Graded microstructure and mechanical properties of additive manufactured Ti–6Al–4V via electron beam melting. *Acta Mater.* **97**, 1–16 (2015). <https://doi.org/10.1016/j.actamat.2015.06.036>

89. Tang, Z.-J., Liu, W., Wang, Y., Saleheen, K., Liu, Z.-C., Peng, S.-T., Zhang, Z., Zhang, H.-C.: A review on in situ monitoring technology for directed energy deposition of metals. *Int. J. Adv. Manuf. Technol.* **108**, (2020). <https://doi.org/10.1007/s00170-020-05569-3>
90. Tapia, G., Elwany, A.: A review on process monitoring and control in metal-based additive manufacturing. *J. Manuf. Sci Eng.* **136**, 060801 (2014). <https://doi.org/10.1115/1.4028540>
91. Thijs, L., Montero Sistiaga, M.L., Wauthle, R., Xie, Q., Kruth, J.-P., Van Humbeeck, J.: Strong morphological and crystallographic texture and resulting yield strength anisotropy in selective laser melted tantalum. *Acta Mater.* **61**, 4657–4668 (2013). <https://doi.org/10.1016/j.actamat.2013.04.036>
92. Tofail, S.A.M., Koumoulos, E.P., Bandyopadhyay, A., Bose, S., O'Donoghue, L., Chari-tidis, C.: Additive manufacturing: scientific and technological challenges, market uptake and opportunities. *Mater. Today* **21**, 22–37 (2018). <https://doi.org/10.1016/j.mattod.2017.07.001>
93. Trevisan, F., Calignano, F., Aversa, A., Marchese, G., Lombardi, M., Biamino, S., Ugues, D., Manfredi, D.: Additive manufacturing of titanium alloys in the biomedical field: processes, properties and applications. *J Appl. Biomater. Funct. Mater.* **16**, 57–67 (2018). <https://doi.org/10.5301/jabfm.5000371>
94. Vilardell, A.M., Yadroitsev, I., Yadroitsava, I., Albu, M., Takata, N., Kobashi, M., Krakhmalev, P., Kouprianoff, D., Kothleitner, G., Plessis, A. du: Manufacturing and characterization of in-situ alloyed Ti6Al4V(EL)-3 at.% Cu by laser powder bed fusion. *Addit. Manuf.* **36**, 101436 (2020). <https://doi.org/10.1016/j.addma.2020.101436>
95. Vilaro, T., Colin, C., Bartout, J.D.: As-Fabricated and heat-treated microstructures of the Ti-6Al-4V Alloy processed by selective laser melting. *Metall Mater Trans A* **42**, 3190–3199 (2011). <https://doi.org/10.1007/s11661-011-0731-y>
96. Wang, J.F., Sun, Q.J., Wang, H., Liu, J.P., Feng, J.C.: Effect of location on microstructure and mechanical properties of additive layer manufactured Inconel 625 using gas tungsten arc welding. *Mater. Sci. Eng. A* **676**, 395–405 (2016). <https://doi.org/10.1016/j.msea.2016.09.015>
97. Wang, P., Tan, X., Nai, M.L.S., Tor, S.B., Wei, J.: Spatial and geometrical-based characterization of microstructure and microhardness for an electron beam melted Ti-6Al-4V component. *Mater. Design.* **95**, 287–295 (2016). <https://doi.org/10.1016/j.matdes.2016.01.093>
98. Wei, H., Wang, L., Niu, X., Zhang, J., Simeone, A.: Fabrication, experiments, and analysis of an LBM additive-manufactured flexure parallel mechanism. *Micromachines* **9**, 572 (2018). <https://doi.org/10.3390/mi9110572>
99. Weingarten, C., Buchbinder, D., Pirch, N., Meiners, W., Wissenbach, K., Poprawe, R.: Formation and reduction of hydrogen porosity during selective laser melting of AlSi₁₀Mg. *J. Mater. Process. Technol.* **221**, 112–120 (2015). <https://doi.org/10.1016/j.jmatprotec.2015.02.013>
100. Xiao, Z., Chen, C., Zhu, H., Hu, Z., Nagarajan, B., Guo, L., Zeng, X.: Study of residual stress in selective laser melting of Ti₆Al₄V. *Mater Design.* **193**, 108846 (2020). <https://doi.org/10.1016/j.matdes.2020.108846>
101. Yadollahi, A., Shamsaei, N.: Additive manufacturing of fatigue resistant materials: challenges and opportunities. *Int. J. Fatigue* **98**, 14–31 (2017). <https://doi.org/10.1016/j.ijfatigue.2017.01.001>
102. Yadollahi, A., Shamsaei, N., Thompson, S.M., Seely, D.W.: Effects of process time interval and heat treatment on the mechanical and microstructural properties of direct laser deposited 316L stainless steel. *Mater. Sci. Eng. A* **644**, 171–183 (2015). <https://doi.org/10.1016/j.msea.2015.07.056>
103. Yamanaka, K., Saito, W., Mori, M., Matsumoto, H., Chiba, A.: Preparation of weak-textured commercially pure titanium by electron beam melting. *Addit. Manuf.* **8**, 105–109 (2015). <https://doi.org/10.1016/j.addma.2015.09.007>
104. Yan, L., Chen, Y., Liou, F.: Additive manufacturing of functionally graded metallic materials using laser metal deposition. *Addit. Manuf.* **31**, 100901 (2020). <https://doi.org/10.1016/j.addma.2019.100901>
105. Yang, T., Liu, T., Liao, W., Wei, H., Zhang, C., Chen, X., Zhang, K.: Effect of processing parameters on overhanging surface roughness during laser powder bed fusion of AlSi₁₀Mg. *J. Manuf. Process.* **61**, 440–453 (2021). <https://doi.org/10.1016/j.jmapro.2020.11.030>

106. Yasa, E., Kempen, K., Kruth, J., Thijs, L., Van Humbeeck, J.: Microstructure and mechanical properties of maraging steel 300 after selective laser melting. In: Solid freeform fabrication symposium proceedings, pp. 383–396 (2010)
107. Yin, J., Yang, L., Yang, X., Zhu, H., Wang, D., Ke, L., Wang, Z., Wang, G., Zeng, X.: High-power laser-matter interaction during laser powder bed fusion. *Addit. Manuf.* **29**, 100778 (2019). <https://doi.org/10.1016/j.addma.2019.100778>
108. Zadi-Maad, A., Rohib, R., Irawan, A.: Additive manufacturing for steels: a review. *IOP Conf. Ser.: Mater. Sci. Eng.* **285**, 012028 (2018). <https://doi.org/10.1088/1757-899X/285/1/012028>
109. Zakirov, A., Belousov, S., Bogdanova, M., Korneev, B., Stepanov, A., Perepelkina, A., Levchenko, V., Meshkov, A., Potapkin, B.: Predictive modeling of laser and electron beam powder bed fusion additive manufacturing of metals at the mesoscale. *Addit. Manuf.* **35**, 101236 (2020). <https://doi.org/10.1016/j.addma.2020.101236>
110. Zhai, Y., Galarraga, H., Lados, D.A.: Microstructure evolution, tensile properties, and fatigue damage mechanisms in Ti-6Al-4V alloys fabricated by two additive manufacturing techniques. *Procedia Eng.* **114**, 658–666 (2015). <https://doi.org/10.1016/j.proeng.2015.08.007>
111. Zhai, Y., Galarraga, H., Lados, D.A.: Microstructure, static properties, and fatigue crack growth mechanisms in Ti-6Al-4V fabricated by additive manufacturing: LENS and EBM. *Eng. Fail. Anal.* **69**, 3–14 (2016). <https://doi.org/10.1016/j.engfailanal.2016.05.036>
112. Zhang, Y., Wu, L., Guo, X., Kane, S., Deng, Y., Jung, Y.-G., Lee, J.-H., Zhang, J.: Additive manufacturing materials: a review. *J. Mater. Eng. Perform.* **27**, 1–13 (2018). <https://doi.org/10.1007/s11665-017-2747-y>
113. Zheng, L., Liu, Y., Sun, S., Zhang, H.: Selective laser melting of Al–8.5Fe–1.3V–1.7Si alloy: investigation on the resultant microstructure and hardness. *Chinese J. Aeronaut.* **28**, 564–569 (2015). <https://doi.org/10.1016/j.cja.2015.01.013>
114. Ziętala, M., Durejko, T., Polański, M., Kuncie, I., Płociński, T., Zieliński, W., Łazińska, M., Stępniewski, W., Czujko, T., Kurzydłowski, K.J., Bojar, Z.: The microstructure, mechanical properties and corrosion resistance of 316L stainless steel fabricated using laser engineered net shaping. *Mater. Sci. Eng. A* **677**, 1–10 (2016). <https://doi.org/10.1016/j.msea.2016.09.028>
115. Microstructural investigation of selective laser melting 316L stainless steel parts exposed to laser re-melting. *Procedia Eng.* **19**, 389–395 (2011). <https://doi.org/10.1016/j.proeng.2011.11.130>
116. Effects of defects in laser additive manufactured Ti-6Al-4V on fatigue properties. *Phys. Procedia*. **56**, 371–378 (2014). <https://doi.org/10.1016/j.phpro.2014.08.120>
117. Additive Manufacturing of Titanium Alloy for Aircraft Components: *Procedia CIRP*. **35**, 55–60 (2015). <https://doi.org/10.1016/j.procir.2015.08.061>
118. Metal powders—the raw materials, <https://www.metal-am.com/introduction-to-metal-additive-manufacturing-and-3d-printing/metal-powders-the-raw-materials/>
119. Standards for metal Additive Manufacturing: A global perspective, <https://www.metal-am.com/articles/standards-for-metal-3d-printing-a-global-perspective/>
120. Electronic Beam Melting, <https://www.whiteclouds.com/3dpedia/ebm.html>
121. ARTICLE: Additive Manufacturing of Aluminum Alloys—Light Metal Age Magazine, <https://www.lightmetalage.com/news/industry-news/3d-printing/article-additive-manufacturing-of-aluminum-alloys/>
122. Additive manufacturing: technology, applications and research needs | SpringerLink, <https://link.springer.com/article/10.1007%2Fs11465-013-0248-8>
123. A Review on Process Monitoring and Control in Metal-Based Additive Manufacturing | *J. Manuf. Sci. Eng.* | ASME Digital Collection, <https://asmedigitalcollection.asme.org/manufacturingscience/article-abstract/136/6/060801/377521/A-Review-on-Process-Monitoring-and-Control-in>
124. Using machine learning to aid in the parameter optimisation process for metal-based additive manufacturing | Emerald Insight, <https://doi.org/10.1108/RPJ-08-2019-0213/full/html>
125. 3D printing: a critical review of current development and future prospects | Emerald Insight, <https://doi.org/10.1108/RPJ-11-2018-0293/full/html>

126. Advanced Machining Processes—Prof. Vijay Kumar Jain—Google Books, https://books.google.co.in/books?hl=en&lr=&id=ufyiV6nEyd4C&oi=fnd&pg=PR9&dq=LBM,+EBM,+and+LMD+advantage+and+disadvantages&ots=vQD071htns&sig=cQAT0ziPygNPIMuEOw7NLnQokRs&redir_esc=y#v=onepage&q&f=false
127. Evaluation of Titanium Alloys Fabricated Using Rapid Prototyping Technologies—Electron Beam Melting and Laser Beam Melting, <https://www.ncbi.nlm.nih.gov/pmc/articles/PMC5448875/>
128. Electron Beam Melting—an overview | ScienceDirect Topics, <https://www.sciencedirect.com/topics/chemistry/electron-beam-melting>
129. Tensile Testing for 3D Printing Materials, <https://www.protolabs.com/resources/blog/tensile-testing-for-3d-printing-materials/>
130. On the mechanical behaviour of titanium alloy TiAl₆V₄ manufactured by selective laser melting: Fatigue resistance and crack growth performance—ScienceDirect, <https://www.sciencedirect.com/science/article/abs/pii/S014211231200343X>
131. Process optimization, microstructures and mechanical properties of a Cu-based shape memory alloy fabricated by selective laser melting—ScienceDirect, <https://www.sciencedirect.com/science/article/abs/pii/S0925838819301616>
132. ARTICLE: Additive Manufacturing of Aluminum Alloys
133. Tensile Testing for 3D Printing Materials